www.nature.com/cdd

CDDpress

ARTICLE

Check for updates

Functional recovery of the germ line following splicing collapse

Wei Cao[1], Christopher Tran[1], Stuart K. Archer[2], Sandeep Gopal[1]✉ and Roger Pocock[1]✉

Splicing introns from precursor-messenger RNA (pre-mRNA) transcripts is essential for translating functional proteins. Here, we report that the previously uncharacterized *Caenorhabditis elegans* protein MOG-7 acts as a pre-mRNA splicing factor. Depleting MOG-7 from the *C. elegans* germ line causes intron retention in most germline-expressed genes, impeding the germ cell cycle, and causing defects in nuclear morphology, germ cell identity and sterility. Despite the deleterious consequences caused by MOG-7 loss, the adult germ line can functionally recover to produce viable and fertile progeny when MOG-7 is restored. Germline recovery is dependent on a burst of apoptosis that likely clears defective germ cells, and viable gametes generated from the proliferation of germ cells in the progenitor zone. Together, these findings reveal that MOG-7 is essential for germ cell development, and that the germ line can functionally recover after a collapse in RNA splicing.

Cell Death & Differentiation (2022) 29:772–787; https://doi.org/10.1038/s41418-021-00891-z

INTRODUCTION

In many species, gametes are produced throughout reproductive life from adult stem cells housed in the germ line. Correct developmental control of germ cell fates is crucial for generating viable gametes and species propagation. As such, mechanisms that control germ cell proliferation, differentiation, survival, and sex determination are directed by highly regulated networks of gene expression.

The *Caenorhabditis elegans* hermaphrodite germ line consists of a pair of U-shaped syncytial tubes organized in a distal-proximal fashion. A population of germline stem cells (GSCs) and their proliferating progeny are located at the distal end of each tube, with mature gametes at their proximal ends. The GSCs reside in a specialized niche supported by Notch signals from somatic cells [1, 2]. GSCs within the niche both self-renew to maintain the stem cell population and produce germ cells that exit the niche and begin the differentiation process. Further proximally, germ cells proceed through meiotic pachytene prior to gametogenesis where they transiently generate sperm from the L3 larval stage, before permanently switching to oogenesis around the L4/adult transition [3]. During the late pachytene phase of the oogenic program, approximately half the germ cells are removed by physiological apoptosis [4]. These apoptosed germ cells are thought to function as nurse cells by providing cytoplasmic components to maturing oocytes [4]. Germ cell apoptosis is also triggered by DNA damage, environmental stress, and pathogen exposure [5–7].

Post-transcriptional gene regulation is critically important for controlling germ cell fates in the *C. elegans* germ line. In particular, precursor-messenger RNA (pre-mRNA) splicing has a strong influence on the transition between germ cell proliferation/differentiation and the sperm-oocyte switch [8, 9]. Splicing of intervening non-coding sequences (introns) from protein-encoding sequences of eukaryotic genes is a highly conserved and complex process (reviewed in [10]). The splicing reaction occurs in a stepwise fashion within a dynamic ribonucleoprotein complex called the spliceosome, containing over 300 proteins in humans [10]. Intron excision occurs in two sequential transesterification reactions that result in the excision of the intron lariat, and the ligation of the 3′ and 5′ exons. The spliceosome is then disassembled, and the lariat released from the intron lariat spliceosome complex (ILS), freeing the spliced mRNA for protein synthesis and enabling the spliceosome complex components and intron nucleotides to be recycled. Spliceosome disassembly is essential for efficient splicing because the spliceosome assembles de novo at each new round of pre-mRNA splicing [11]. Splicing factors, encoded by *mog* genes (masculinization of the germ line), promote *C. elegans* oogenesis: their depletion causes a failure in the sperm-oocyte switch and the generation of a germ line replete with sperm (spermatogenic germ line) [12, 13]. The switch from spermatogenesis to oogenesis is controlled by many RNA regulatory proteins that comprise the germ line sex determination pathway [14]. It is thought that inefficient splicing of these sex determining genes caused by mutations in *mog* genes inhibits appropriate switching of sexual fate in the germ line [8].

Here, we determined the function of the previously uncharacterized gene *mog-7* in the *C. elegans* germline. The *mog-7* locus encodes two protein isoforms: a long isoform containing a *Saccharomyces cerevisiae* Ntr2 (Nineteen Complex-Related Protein 2) domain and a human GCFC (GC-rich sequence DNA-binding factor) domain, and a short isoform containing only the GCFC domain. Ntr2 and GCFC domains are found in factors that regulate the disassembly of the ILS by the DEAH family ATPase/helicase Prp43 [15, 16]. We found that MOG-7 is expressed throughout the germ line and that germline-specific removal of MOG-7 inhibits germline development and causes complete sterility; likely due to abnormalities observed in nuclear morphology and the germ cell cycle. We found that MOG-7 interacts in vivo with multiple splicing

[1]Development and Stem Cells Program, Monash Biomedicine Discovery Institute and Department of Anatomy and Developmental Biology, Monash University, Melbourne, VIC 3800, Australia. [2]Monash Bioinformatics Platform, Monash University, Melbourne, VIC 3800, Australia. ✉email: sandeep.gopal@monash.edu; roger.pocock@monash.edu

Edited by E. Baehrecke

Received: 10 June 2021 Revised: 30 September 2021 Accepted: 4 October 2021
Published online: 18 October 2021

factors required for spliceosome disassembly. Moreover, germline-specific removal of MOG-7 causes intron retention in over 5000 germline-expressed genes. Despite the severe defects in RNA splicing and germ cell behavior, the germ line can recover from MOG-7 depletion to produce viable and fertile progeny if MOG-7 expression is restored. We observed a burst of apoptotic death in the germ line within hours of restoring MOG-7 expression, and recovery of germline function is dependent on the apoptotic caspase CED-3. Therefore, removal of defective germ cells is required for germline recovery following restoration of MOG-7 expression. In addition, germline recovery from splicing collapse requires proliferation, likely from a cohort of arrested distal germ cells. Together, we demonstrate that the *C. elegans* germ line exhibits a capacity to functionally recover following a catastrophic breakdown of RNA splicing.

RESULTS

F43G9.12/MOG-7 is essential for *C. elegans* germline development

In an ongoing RNA-mediated interference (RNAi) screen for nucleic acid binding factors that control germline development, we identified the uncharacterized gene *F43G9.12/mog-7*. The *mog-7* locus generates two protein isoforms—MOG-7a and MOG-7b (Fig. 1A). MOG-7a contains Ntr2 and GCFC domains, with MOG-7b housing the GCFC domain alone (Fig. 1A). Proteins containing these domains have been shown to independently control splicing in *Saccharomyces cerevisiae* (Ntr2) and humans (GCFC—also known as C2orf3) [15, 17, 18].

We explored the function of *mog-7* in the germ line by RNAi targeting of both isoforms (Fig. 1A, B and Supplementary Fig. S1). *mog-7* RNAi knockdown from the L1 larval stage induced a spermatogenic germ line in approximately 35% of P0 animals (Fig. 1B and Supplementary Fig. S1A). This phenotype corresponds with other studies of splicing factors in the *C. elegans* germ line that also control the sperm-oocyte switch [8, 12, 13, 19–21]. *mog-7* L1 RNAi also resulted in low broods with most F1 progeny dying during embryogenesis (Supplementary Fig. S1B). *mog-7* RNAi from the L4 larval stage enabled hermaphrodites to generate more progeny than L1 knockdown; however, few embryos hatched into larvae (Supplementary Fig. S1C). Thus, *mog-7* is critical for fertility and embryonic viability.

MOG-7 autonomously controls germline development

To examine the endogenous expression pattern of MOG-7, we used CRISPR-Cas9 to knock-in a *degron::green fluorescent protein* (*gfp)* coding sequence at the 3′ end of the *mog-7* gene, thereby tagging both MOG-7 isoforms (Fig. 1C) [22]. We inserted the degron sequence to enable acute removal of endogenous MOG-7 using the auxin-inducible degron (AID) system [23]. MOG-7::degron::GFP expression was detected in germline nuclei throughout development, commencing in the primordial germ cells of L1 larvae through to oocytes and sperm in adults (Fig. 1D, E and Supplementary Fig. S2). Somatic expression of MOG-7::degron::GFP was detected in embryos from the 2-cell stage and throughout worm development in most, if not all, cells (Supplementary Fig. S2). MOG-7::degron::GFP expression was also detected by western blot confirming the presence of both MOG-7 isoforms (Supplementary Fig. S2F). We found that insertion of the degron::GFP sequence had no overt effect on MOG-7 germline function as shown by germ cell counting and brood size analysis (Supplementary Fig. S3). In addition, incubating animals on auxin-containing media did not affect germ cell number (Supplementary Fig. S3).

To validate the efficacy of the MOG-7::degron::GFP allele for functional studies, we introduced a transgene that expresses the *Arabidopsis thaliana* F-box protein called transport inhibitor response 1 (TIR1) in the germ line (*sun-1p::TIR1::mRuby*) of *mog-7::degron::gfp* animals [23]. In the presence of auxin, TIR1 targets AID-tagged proteins for ubiquitin-dependent proteasomal degradation [23]. The *sun-1p::TIR1::mRuby* transgene had no detectable effect on germline function either alone or in the presence of *mog-7::degron::gfp* (Supplementary Fig. S3). We found that exposing *mog-7::degron::gfp; sun-1p::TIR1::mRuby* adult hermaphrodites to auxin for 1 h depleted MOG-7::degron::GFP specifically in the germ line, without detectable changes in the soma (Fig. 1E and Supplementary Fig. S3E). Therefore, MOG-7::degron::GFP can be rapidly removed using the AID system.

Our initial RNAi analysis showed that *mog-7* knockdown causes defects in germ cell fate and fecundity (Fig. 1B and Supplementary Fig. S1). However, this phenotype may be caused by a non-autonomous function for *mog-7* from somatic tissue. As we observed germline-specific loss of MOG-7::degron::GFP expression in *mog-7::degron::gfp; sun-1p::TIR1::mRuby* animals following auxin exposure (called MOG-7 AID from here) (Fig. 1E and Supplementary Fig. S3E), we used this tool to examine the autonomous role of *mog-7* in the germ line. *mog-7* RNAi from the L1 larval stage caused a spermatogenic germ line in ~35% of animals (Fig. 1B and Supplementary Fig. S1A). As spermatogenesis begins in late L3 larvae [24], we performed continuous MOG-7 AID from this stage and found that ~80% of animals had spermatogenic germ lines in the first day of adulthood (Fig. 1F). In contrast, MOG-7 AID from the early L4 stage (6 h after late L3) resulted in mostly oogenic germ lines (Fig. 1F). This reveals the importance of MOG-7 in determining the sexual fate of germ cells before the L4 stage. Next, we determined the effect of MOG-7 AID on fecundity after the sperm-oocyte switch with continuous auxin treatment from the early L4 stage. We found that all MOG-7 AID animals were sterile, indicating a severe defect in germline health (Fig. 1G). The germ cell fate and fecundity phenotypes caused by MOG-7 AID were stronger than in our RNAi experiments, likely because RNAi does not completely remove *mog-7* mRNA. Taken together, these data show that MOG-7 is a critical, autonomous regulator of germline development.

MOG-7 is acutely required to maintain germ cell health

We next explored the cellular basis of germline sterility caused by MOG-7 AID. To dissect the function of MOG-7 in regulating germ cell behavior, we grew hermaphrodites to 1-day adults and then performed MOG-7 AID for 6 h. We then extracted germ lines and examined germ cell nuclear morphology by staining DNA with 4′,6-diamidino-2-phenylindole (DAPI) (Fig. 2A–C). In the progenitor zone (PZ), we observed multiple germ cells with bright florets of DAPI-stained DNA, some of which contain large nuclei that suggest arrest in the G2 phase of the cell cycle prior to mitotic division (Fig. 2A) [25]. The transition zone is normally dominated by nuclei in early meiotic prophase, which have a crescent-shaped chromosome morphology indicative of meiotic chromosome pairing [26]. We found that MOG-7 AID caused severe defects in germ cell morphology such that few crescent-shaped nuclei were recognizable, suggesting defects in chromosome packaging (Fig. 2B). As germ cells advance into the pachytene region, synapsed homologous chromosomes form compact ribbons (Fig. 2C). After MOG-7 depletion, pachytene nuclei are spatially disorganized and have irregular morphology (Fig. 2C). Together, these data reveal that depletion of *mog-7* causes defects in germ cell nuclear morphology throughout the germ line.

We next examined whether MOG-7 depletion affects germ cell behavior by examining the cell cycle (Fig. 2D–J). To assess the proliferative state of PZ cells after MOG-7 AID, we detected cells in M-phase by staining germ lines with an antibody against phospho-histone H3 (pH3) (Fig. 2E, F). We found that the number of M-phase cells in adult germ lines was significantly reduced compared to control after 1 h of MOG-7 AID (Fig. 2F). After 2 h of MOG-7 AID, approximately half the number of control pH3-

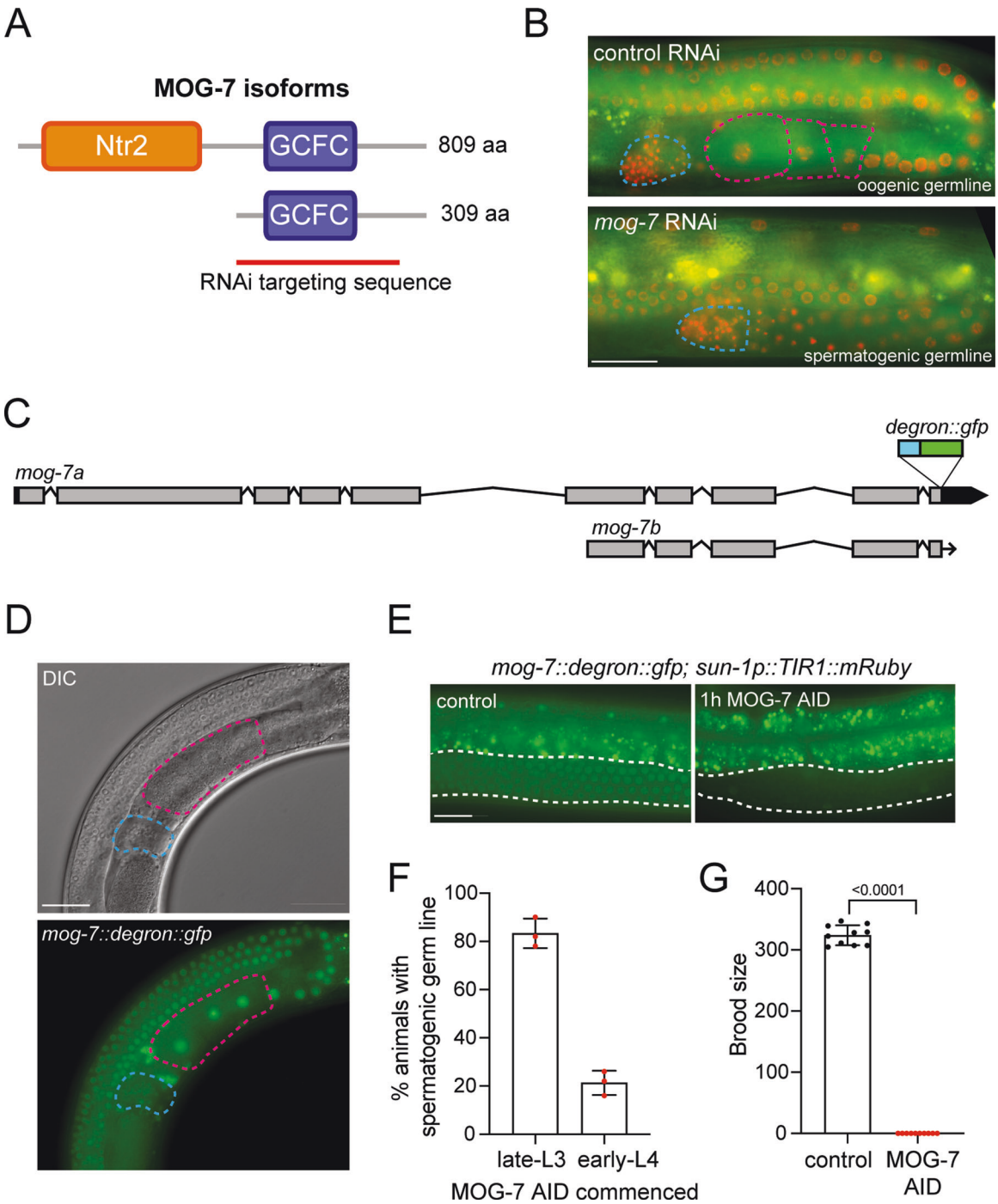

Fig. 1 MOG-7 controls germ cell fate and fertility. A Protein domain of MOG-7a and MOG-7b. Ntr2, Nineteen complex-related protein 2, pre-mRNA splicing factor domain. GCFC, GC-rich sequence DNA-binding factor 2 domain. Red line = targeting sequence in RNAi experiments. **B** Fluorescence micrographs of one-day adult germ lines +/− *mog-7* RNAi from the L1 larval stage (control = L4440 vector). Micrographs show chromosomes in red (mCherry::HIS-58) and plasma membrane in green (GFP::PH(PLC1delta1)) [54]. Spermatheca = blue dashes. Oocytes = pink dashes. Scale bar = 20 µm. **C** *mog-7* genomic structure showing the insertion site of the *degron::gfp* coding sequence at the C-terminus of both isoforms. **D** Differential interference contrast (DIC) and fluorescence micrographs of *mog-7::degron::gfp* expression in an adult hermaphrodite. Spermatheca = blue dashes. Oocytes = pink dashes. Scale bar = 20 µm. **E** Fluorescence micrographs of *mog-7::degron::gfp* expression +/− auxin treatment for 1 h (ethanol used as a control). *sun-1p::TIR1::mRuby* = germline-specific auxin-inducible degron strain. Dashed line = germ line region. Scale bar = 10 µm. **F** Percentage of spermatogenic adult hermaphrodite germ lines of *mog-7::degron::gfp; sun-1p::TIR1::mRuby* exposed to auxin from the late-L3 or late-L4 stage. Data expressed as mean ± SEM and statistical significance was assessed by Welch's *t*-test. $n = 40$ per replicate. **G** Quantification of brood size of *mog-7::degron::gfp; sun-1p::TIR1::mRuby* hermaphrodites exposed to ethanol or auxin from the early L4 stage. Data expressed as mean ± SEM and statistical significance was assessed by Welch's *t*-test. $n = 10$.

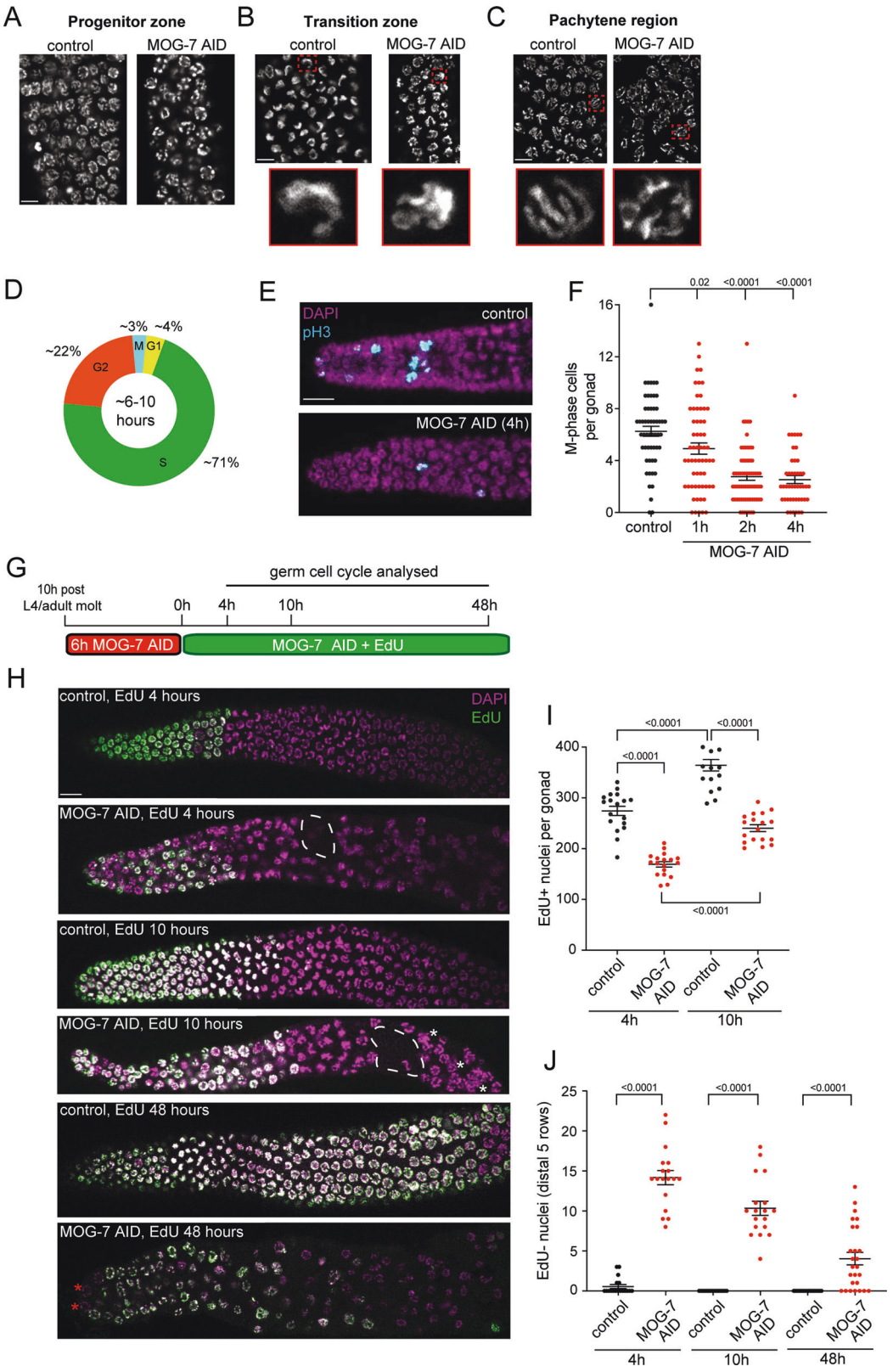

positive nuclei were detected and this level remained unchanged after 4 h, suggesting reduced/slowing in proliferation (Fig. 2F).

To provide more granularity to potential cell cycle alterations caused by MOG-7 AID, we labeled S-phase germ cells in the PZ with the thymidine analog 5-ethynyl-2′-deoxyuridine (EdU) in a time-course experiment (Fig. 2G). To examine the ability of MOG-7-depleted germ cells to enter S-phase, we exposed 1-day adults (10 h after the L4/adult molt) to MOG-7 AID for 6 h, and then supplied EdU for 4, 10, and 48 h while maintaining MOG-7 depletion (Fig. 2G–J). After 4 and 10 h of EdU treatment, we

Fig. 2 MOG-7 depletion causes defects in nuclear morphology and germ cell behavior. A–C DAPI-stained germ cell nuclei in the progenitor zone (**A**), transition zone (**B**), pachytene region (**C**) of *mog-7::degron::gfp; sun-1p::TIR1::mRuby* 1-day adult hermaphrodites exposed to ethanol or auxin for 6 h. Hatched red boxes highlight individual nuclei magnified below where appropriate. Scale bars = 5 µm. **D** Schematic of germ cell cycle length and percentage of germ cells at each cell cycle stage in an adult hermaphrodite (taken from [40]). **E**, **F** Fluorescence micrographs (**E**) and quantification (**F**) of M-phase cells in distal germ lines of *mog-7::degron::gfp; sun-1p::TIR1::mRuby* 1-day adult hermaphrodites exposed to ethanol or auxin for 1, 2, and 4 h. Germ lines stained with DAPI to visualize DNA (magenta) and anti-phospho-histone H3 (pH3) to visualize M-phase chromosomes (cyan). Data expressed as mean ± SEM and statistical significance was assessed by one-way ANOVA multiple comparison with Sidak correction. $n = 45$. Scale bar = 10 µm. **G** Experimental outline for S-phase labeling of adult germ cells following *mog-7* depletion; 10 h after the L4/adult molt, *mog-7::degron::gfp; sun-1p::TIR1::mRuby* hermaphrodites were continuously incubated on auxin or ethanol plates. After 6 h of MOG-7 AID, animals were labeled with 5-ethynyl-2′-deoxyuridine (EdU) by feeding for 4, 10, and 48 h, and germ lines extruded and analyzed. Control animals were exposed to ethanol for the same periods. **H** Fluorescence micrographs of *mog-7::degron::gfp; sun-1p::TIR1::mRuby* 1-day adult control and MOG-7 AID hermaphrodites labeled with EdU for 4, 10, and 48 h. Germ lines stained with DAPI to visualize DNA (magenta) and labeled with EdU to detect replicated DNA (green). Areas devoid of germ cells = white dashed area. Nuclei clusters = white asterisks. EdU-negative (EdU^-) nuclei = red asterisks. Scale bar = 10 µm. **I** Quantification of EdU^+ nuclei in *mog-7::degron::gfp; sun-1p::TIR1::mRuby* 1-day adult hermaphrodites exposed to ethanol or auxin for 4 and 10 h. Data expressed as mean ± SEM and statistical significance was assessed by one-way ANOVA multiple comparison with Sidak correction. $n = 17–18$. **J** Quantification of EdU^- nuclei in *mog-7::degron::gfp; sun-1p::TIR1::mRuby* 1-day adult hermaphrodites exposed to ethanol or auxin for 4, 10, and 48 h. Data expressed as mean ± SEM and statistical significance was assessed by one-way ANOVA multiple comparison with Sidak correction. $n = 17–18$.

observed fewer EdU^+ cells in MOG-7 AID germ lines compared to control animals, suggesting a slowing of the cell cycle (Fig. 2H, I). However, there was a significant increase in EdU^+ cells between 4 and 10 h in MOG-7 AID germ lines indicating that germ cells can still enter S-phase (Fig. 2I). We also observed areas of the germ line that were devoid of nuclei and the presence of nuclei clusters, revealing that the organization of germ cells through the germ line is perturbed (Fig. 2H). We next examined S-phase entry of PZ germ cells in the five most distal rows that house the GSCs (Fig. 2J) [27]. In control animals, all distal germ cells are labeled with EdU within 10 h (most are in fact labeled within 4 h) (Fig. 2J). However, in MOG-7 AID animals, 10–15 germ cells are EdU^- after 10 h of EdU labeling (Fig. 2J). Even after 48 h of EdU incubation, some germ cells were not labeled with EdU (Fig. 2H, J). Thus, germ cells in the PZ respond to MOG-7 depletion by slowing the cell cycle, with a cohort of germ cells arresting prior to S-phase. Taken together, these data reveal that MOG-7 AID causes diverse defects in germ cell behavior and morphology throughout the germ line that likely account for the sterility phenotype.

MOG-7 interacts with multiple pre-mRNA splicing factors

To explore how MOG-7 controls germ cell behavior, we identified MOG-7::degron::GFP in vivo interacting proteins by immunoprecipitation (IP) and mass spectrometry (MS) (Fig. 3A). We identified five candidate proteins that interact with MOG-7::degron::GFP in each of three independent MS experiments (Fig. 3B and Supplementary Table S1). Intriguingly, 4/5 candidate MOG-7 interactors are part of the ILS complex in *S. cerevisiae* (EFTU-2/Snu114p, PRP-8/Prp8p, STIP-1/Ntr1p and SKP-1/Prp45p), and one is uncharacterized (Y94H6A.3) (Fig. 3B) [28]. To confirm the interactions identified by MS analysis, we performed independent co-immunoprecipitation experiments where V5-tagged MOG-7a or MOG-7b were co-expressed in COS-7 cells with each candidate interacting protein fused to a FLAG tag (Fig. 3C, Supplementary Fig. S4, and Supplementary Table S1). We confirmed that FLAG-tagged EFTU-2, PRP-8, STIP-1, and SKP-1 interact with both MOG-7 isoforms, whereas an interaction was only detected between Y94H6A.3 and MOG-7a-V5 (Fig. 3C and Supplementary Table S1). One of the MOG-7 interactors we identified called SKP-1 is a component of the PRP19 NTC-related (NTR) complex that is essential for catalyzing spliceosome disassembly (Fig. 3B, C) [29]. We found that both MOG-7 isoforms also interact with PRP-19 in mammalian cells suggesting a function for MOG-7 in controlling spliceosome disassembly (Fig. 3C and Supplementary Table S1). In *S. cerevisiae*, the Ntr2 protein interacts with Ntr1 (STIP-1 in *C. elegans*) within the ILS [28]. We therefore wondered whether the Ntr2 domain of MOG-7a can independently interact with the ILS components we detected by MS. We therefore removed the GCFC domain from MOG-7a and co-expressed the Ntr2 domain with the ILS complex proteins (Fig. 3D and Supplementary Fig. S4). We found that the Ntr2 domain of MOG-7a can interact with these proteins (Fig. 3D and Supplementary Fig. S4). Together, these data reveal that both the Ntr2 and GCFC domains of MOG-7 interact with multiple proteins involved in spliceosome disassembly, suggesting a function for MOG-7 in this process.

Acute loss of MOG-7 causes intron retention

MOG-7a contains Ntr2 and GCFC domains that regulate spliceosome disassembly in *S. cerevisiae* and humans, respectively [15, 18]. In addition, we have shown that both MOG-7 isoforms interact in vivo with multiple proteins that control lariat intron release and spliceosome disassembly (Fig. 3). As recycling of these spliceosome components is a pre-requisite for each new round of splicing [11], we hypothesized that MOG-7 is important for efficient splicing in the *C. elegans* germline. To examine the impact of acute MOG-7 AID depletion on the transcriptome, we performed germline-specific MOG-7 AID on synchronized young adult hermaphrodites (prior to formation of embryos) for 1 or 2 h followed by whole-animal RNA sequencing (Fig. 4A, see Methods for detailed protocol). Ethanol treatment for 2 h was used as a control. We have shown that within 1 h of AID, MOG-7::degron::GFP protein is undetectable and germline phenotypes are detected (Figs. 1 and 2). Therefore, we predicted that the potential detrimental effect of MOG-7::degron::GFP loss on the transcriptome could be detected within 1 h of MOG-7 depletion. Six replicates of each treatment were collected for RNA extraction and sequencing. Multi-dimensional scaling analysis shows that each treatment group clusters together and independently of each other (Supplementary Fig. S5A).

We first examined exonic sequences to identify differentially expressed genes (DEGs) (Supplementary Fig. S5B, D and Supplementary Table S2). There were 243 and 702 DEGs (FDR < 0.05, absolute logFC > 0.585) identified after 1 and 2 h of MOG-7 AID, respectively, with an overlap of 182 genes. Many of the DEGs identified were not germline-expressed genes (45% of 1 h MOG-7 AID genes and 34% of 2 h MOG-7 AID genes) (Supplementary Fig. S5B, D). As we performed germline-specific MOG-7 AID, we supposed somatic DEGs may be responding to the auxin treatment rather than MOG-7 depletion. We subjected these DEGs to Gene Ontology (GO) overrepresentation analysis according to classification by molecular function and biological process using DAVID (https://david.ncifcrf.gov/). We detected an overrepresentation of GO terms related to xenobiotic stimuli and detoxification pathways, likely indicating responses to auxin exposure (Supplementary Fig. S5E–H and Supplementary Table S2).

A

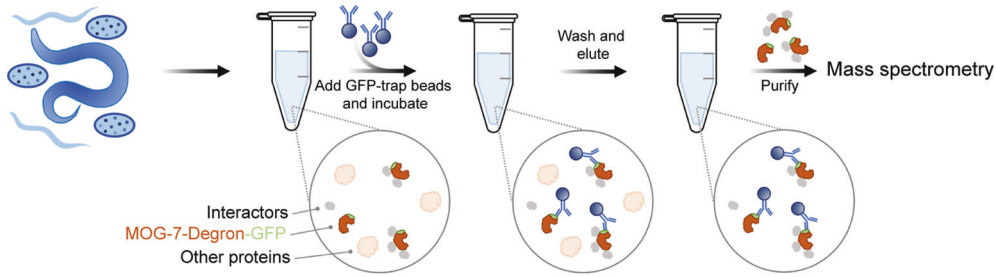

B

C. elegans	*H. sapiens*	*S. cerevisiae*	Function
EFTU-2	U5-116kD/EFTUD2	Snu114	Component of U5 snRNP complex, interacts with PRP8
PRP-8	U5-22-kD/PRPF8	Prp8	Component of U5 snRNP complex, interacts with EFTUD2
STIP-1	TFIP11/NTR1	Ntr1	Recruits PRP43 for lariat intron release and splicesome dissasembly
SKP-1	SNW1	Prp45	Component of PRP19 (NTC) complex
Y94H6A.3	-	-	Unknown

C

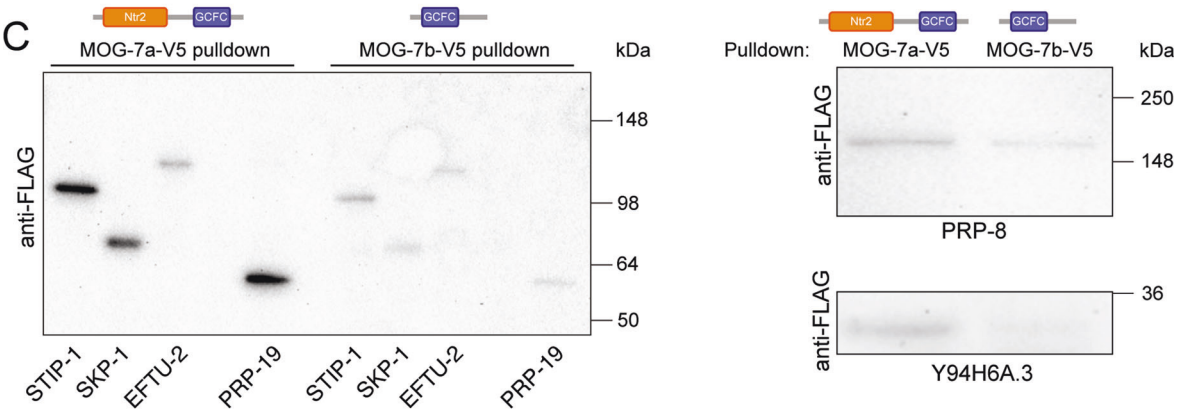

D

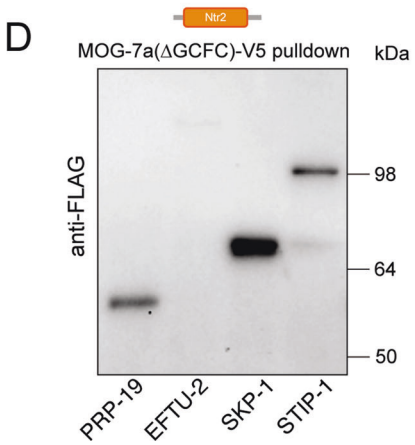

However, we also found overrepresentation of GO terms relating to meiotic chromosome separation, DNA damage, and transcription in the 2 h MOG-7 AID dataset, suggesting that these genes are responding to MOG-7 depletion and/or the associated germline defects (Supplementary Fig. S5G, H).

Due to the predicted function for the MOG-7 protein domains in pre-mRNA splicing, we assessed the effect of germline-specific MOG-7 AID on intron retention (Fig. 4, Supplementary Fig. S6, and Supplementary Table S3). Focusing on the 1 h MOG-7 AID dataset, we identified 5014 genes with retained introns, 93% of which are

Fig. 3 MOG-7 interacts with specific spliceosome proteins. A MOG-7::degron::GFP was immunoprecipitated from adult hermaphrodites, L1 larvae, and embryos using magnetic beads coated with GFP-Trap. Samples were washed to remove proteins not interacting with MOG-7::degron::GFP and then analyzed by mass spectrometry after trypsin digestion. Three independent experiments were performed. **B** Proteins that reproducibly associated with MOG-7::degron::GFP in mass spectrometry experiments were core spliceosome components (EFTU-2, PRP-8, SKP-1), a spliceosome disassembly component (STIP-1), and an uncharacterized protein (Y94H6A.3). Orthologs (*H. sapiens* and *S. cerevisiae*) and known functions of these proteins are shown. **C**, **D** Immunoprecipitation of MOG-7a and MOG-7b (**C**) or MOG-7a(ΔGCFC) (**D**) followed by western blot in COS-7 cells confirming the interaction of both MOG-7 isoforms with spliceosome proteins identified by mass spectrometry ($n \geq 2$ independent experiments). Proteins sizes as marked: FLAG-STIP-1 (94kD), FLAG-PRP-8 (272kD), FLAG-EFTU-2 (110kD), FLAG-Y94H6.A3 (21kD), FLAG-SKP-1 (60kD), FLAG-PRP-19 (53kD). Detailed analysis of interactions is in Supplementary Table S1.

germline-expressed (Fig. 4B). We found that MOG-7 AID increased the global proportion of non-exonic RNA (intronic/intergenic) from autosomes (Fig. 4C and Supplementary Fig. S6). The fact that the greatest difference was observed in low-coverage loci (less than 0.001 per million mapped bases) indicates that most of these differentially expressed regions are not un-annotated exons but rather bona-fide introns or intergenic loci. Global changes in the proportion of non-exonic and exonic RNA were not observed for genes located on the X chromosome, probably due to the low level of transcription on the X chromosome in the germ line [30]. We next examined intron reads per gene compared to expression level and found that as one may predict, genes with more transcripts have more remaining introns (Fig. 4D and Supplementary Fig. S5B). We randomly selected two germline-expressed genes (*cls-2* and *klp-7*) to visualize intron retention caused by MOG-7 AID at specific loci (Fig. 4E). We found that all introns of these genes exhibit a degree of intron retention following 1 h of MOG-7 AID (Fig. 4E). We validated the retention of a specific intron at each of these loci by PCR from independently isolated RNA samples for 1 and 2 h MOG-7 AID (Fig. 4F). Together, these data show that acute loss of MOG-7 from the germ line causes widespread deficits in pre-mRNA splicing, which likely cause germ cell behavioral defects and germline sterility.

The germ line recovers functionality when MOG-7 expression is restored

We have shown that germline depletion of MOG-7 causes developmental delay, sterility, failure of the sperm-oocyte switch, and attenuation of cellular processes such as DNA synthesis, cell cycle progression, proliferation, and nuclear organization (Figs. 1 and 2). These striking phenotypes are consistent with the splicing defects observed in thousands of germline-expressed genes when MOG-7 is depleted (Fig. 4).

Our germ cell analysis identified a cohort of arrested germ cells following long-term MOG-7 depletion (Fig. 2). We therefore wondered whether the germ line has the capacity to recover from such a severe breakdown in splicing and fundamental cellular processes. To examine this question, we used the flexibility of the AID system to monitor germline development after resupplying MOG-7 expression in adults. A previous study showed that protein expression recovers after auxin removal, with the rate of recovery dependent on the concentration of auxin used and potentially the developmental stage of auxin treatment [23]. Furthermore, protein recovery dynamics are dependent on gene-specific transcription and translation rates. To examine the dynamics of MOG-7::degron::GFP expression, we imaged hermaphrodite germ lines after 1 h of auxin exposure and again 1–2 h after auxin removal (Supplementary Fig. S7). We found that MOG-7::degron::GFP expression was undetectable in the germ line after 1 h of auxin exposure and robust expression was restored within the first hour of removal from auxin plates (Supplementary Fig. S7).

Based on the ability of MOG-7 expression to rapidly recover following auxin removal, we established a protocol to examine the effect of restoring MOG-7 expression on germline function (Fig. 5A). We performed germline-specific MOG-7 AID for 18 h from the early L4 stage until the first day of adulthood and then recovered animals on auxin-negative plates (Fig. 5A, B). We compared the brood size of these animals to those exposed to continual germline-specific MOG-7 AID and control animals (ethanol-treated for the same period) (Fig. 5B). We found that as shown in Fig. 1G, animals exposed to continual MOG-7 AID were sterile (Fig. 5B). When we examined the broods of animals in recovery following MOG-7 AID for 18 h, we observed few offspring during the first 2 days of adulthood (Fig. 5B). However, progeny production significantly recovered in 3-day adults and recovered hermaphrodites produced more progeny than control animals between days 4 and 6 (Fig. 5B). In total, MOG-7 AID recovered hermaphrodites generated a mean of 201 viable progeny (SD = 54.79) and 22 dead embryos (SD = 12), compared to control animals that generated a mean of 324 viable progeny (SD = 16.45) and 3 dead embryos (SD = 2). We wondered whether surviving progeny of MOG-7 AID recovered hermaphrodites were viable and fertile. From 56 randomly selected surviving L1 progeny of MOG-7 AID recovered adults, 54 developed into fertile adults, 1 was sterile, and 1 was male. These data show that the germ line can functionally recover following restoration of MOG-7 expression.

How is the adult germ line able to functionally recover from the extensive molecular and cellular deficits caused by MOG-7 depletion? We have shown that few offspring are generated in the first 2 days after restoring MOG-7 expression (Fig. 5B). As it takes approximately 2 days for PZ germ cells to develop into oocytes [31], we reasoned that this period may be utilized to remove defective germ cells from the germline. Indeed, programmed cell death (apoptosis) was previously shown to be required for the regenerative capacity of the germ line following extended starvation [32]. To explore this hypothesis, we performed MOG-7 AID for 18 h from early L4 larvae to young adult, and quantified apoptosis by SYTO-12 staining for 36 h at 6-h intervals following auxin removal (Fig. 5C, D). We observed a large increase in the number of apoptotic cells between 18 and 30 h after auxin removal, with a peak increase of 20-fold compared to control animals at the 24 h time-point (Fig. 5D). Apoptosis functions as part of the physiological oogenesis program to control germ cell number and also facilitates germ cell death in response to DNA damage, environmental stress, and pathogen exposure through distinct molecular pathways [4–7]. These pathways converge at the CED-3 executioner caspase that is essential for germline apoptosis [4]. We found that *ced-3* RNAi abrogates the burst of apoptosis in animals recovering from MOG-7 depletion (Fig. 5E). Conserved proteins acting upstream of CED-3 regulate physiological (LIN-35/Retinoblastoma) and DNA damage-induced (CEP-1/p53) apoptosis [33, 34]. Two BH3-only EGL-1 and CED-13 proteins also act downstream of CEP-1 to promote DNA damage-induced apoptosis through partially parallel mechanisms [35]. To determine the genetic pathway acting upstream of *ced-3* for induction of germ cell apoptosis in MOG-7 AID recovered germlines, we examined genetic mutants of these apoptosis pathway genes (Fig. 5F). As *cep-1* and *mog-7* are closely linked on chromosome I, we used the CRISPR-based STOP-IN method to introduce multiple stop codons into both the long *cep-1* isoform and multiple short *cep-1* isoforms of

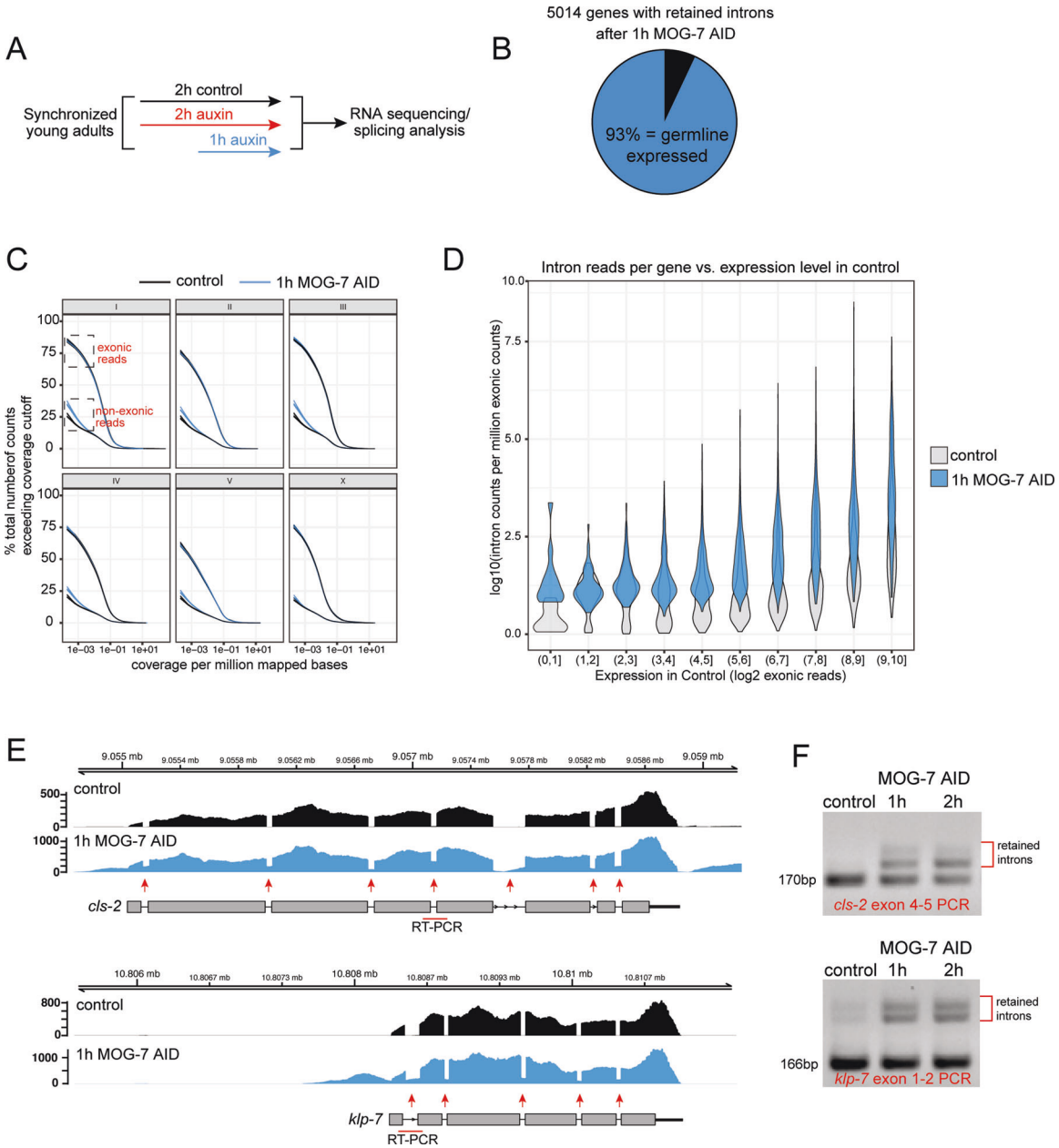

Fig. 4 Acute loss of MOG-7 disrupts RNA splicing. A Experimental summary of *mog-7* depletion for RNA sequencing and splicing analysis. A population of synchronized young adult *mog-7::degron::gfp; sun-1p::TIR1::mRuby* hermaphrodites (with no embryos) were divided into three groups. Two groups were incubated either on ethanol (control) or 1 mM auxin for 2 h. After 1 h, the remaining group was incubated on 1 mM auxin for 1 h. Six replicates of each sample were prepared for RNA sequencing and splicing analysis. **B** Summary of the number of protein-coding genes with retained introns after germline-specific MOG-7 AID (1 h auxin treatment) compared to the ethanol-treated control. Intron-overlapping RNA-seq reads were aggregated at the gene level followed by analysis using EdgeR QL (Methods) with an FDR cutoff of 0.001. **C** Percentage of exonic and non-exonic base-positions (vertical axis) exceeding any given coverage-level threshold (horizontal axis) in each chromosome. Each base-position's coverage-level was normalized by dividing it by the number of millions of read-bases mapped to that chromosome, separately for exonic and non-exonic bases. Six independent replicates of control (ethanol-treated, black lines) and MOG-7 AID (auxin-treated for 1 h, blue lines) treatment groups were plotted. Dashed black boxes highlight exonic and non-exonic counts at the lower coverage threshold region of the plot, where the difference between treated and untreated samples in terms of non-exonic base-position coverage was most apparent. **D** Violin plot showing relative intronic read counts (vertical axis) vs. expression level of host genes (horizontal axis). Black: control (ethanol-treated); blue: MOG-7 AID (1 h auxin treatment). **E** Visualization of splicing analysis of RNA-sequencing data comparing control (ethanol-treated) and MOG-7 AID (1 h auxin treatment). Tracks are shown for selected genes *cls-2* and *klp-7* and are representative of all six replicates per condition. Red arrows indicate retained introns and red lines indicate the amplicon for RT-PCR validation of intron retention shown in (**F**). **F** RT-PCR validation of retained introns for *cls-2* (exon 4-5 PCR) and *klp-7* (exon 1-2 PCR) after MOG-7 AID for 1 and 2 h. Position of the PCR primers used are shown in (**E**) in red beneath schematic showing gene structure. Length of the spliced PCR product indicated in base pairs (bp).

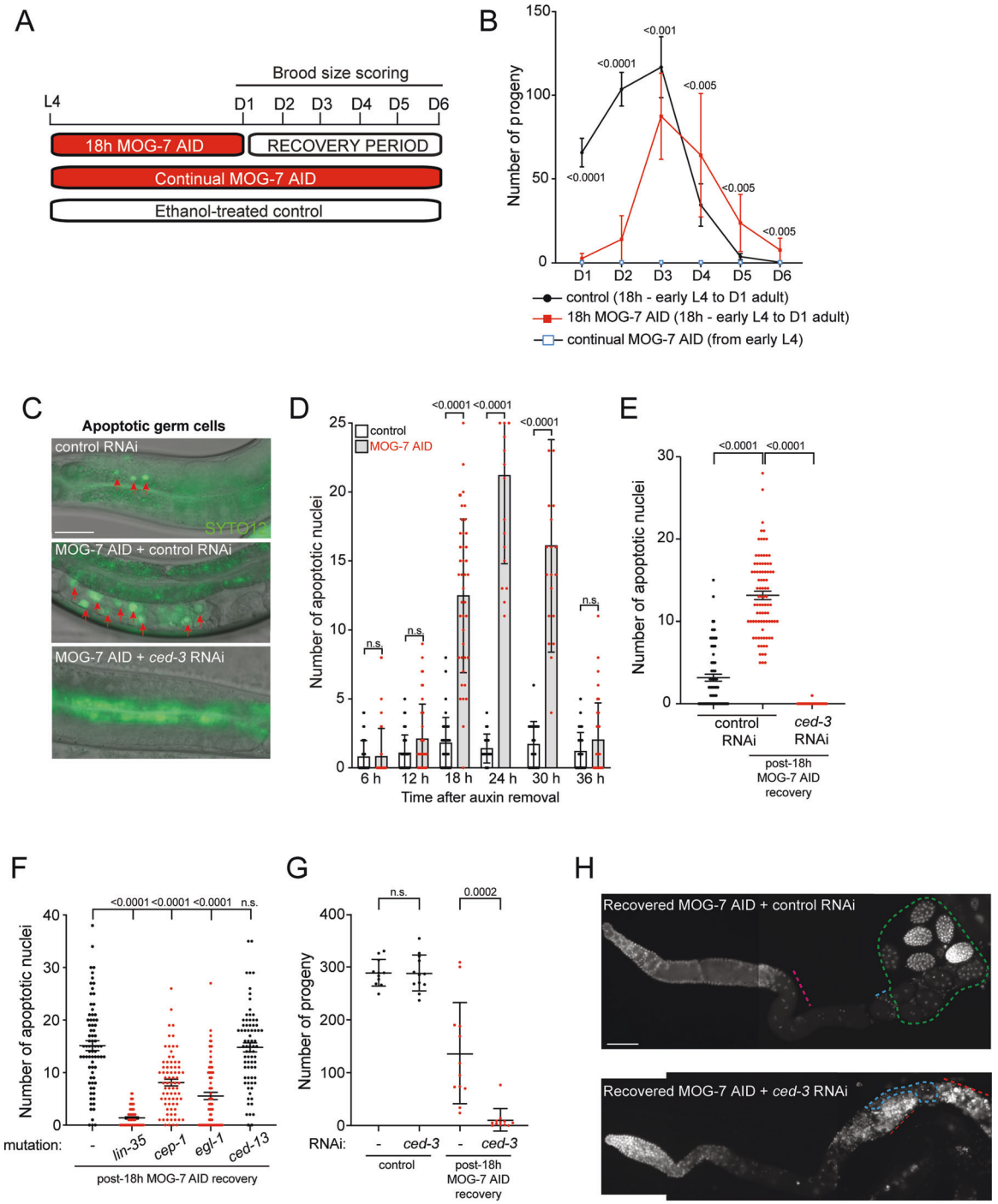

mog-7::degron::gfp; sun-1p::TIR1::mRuby animals (Supplementary Fig. S8) [36]. Our analysis shows that germ cell apoptosis in MOG-7 AID recovered germlines partially requires *lin-35*, *cep-1* and *egl-1* but not *ced-13* (Fig. 5F). This suggests that apoptotic removal of defective germ cells in MOG-7 depleted germ lines is triggered by partially parallel pathways.

The data above suggest that apoptotic clearance of defective germ cells is a pre-requisite for functional recovery of the germ line. We therefore measured the brood size of *ced-3* RNAi knockdown hermaphrodites following recovery from MOG-7 depletion (Fig. 5G). *ced-3* knockdown abolished the ability of the germ line to recover from MOG-7 AID, whereas *ced-3* RNAi animals exposed to ethanol had indistinguishable broods from RNAi control animals (Fig. 5G). DAPI staining of extruded germ lines 48 h after MOG-7 AID recovery detected oocytes and multiple developing embryos in control RNAi animals (Fig. 5H, top panel). In contrast, germ lines of *ced-3* RNAi animals were severely disorganized with defective gametes and masses of proximal DAPI staining, likely representing endomitotic nuclei (Fig. 5H, bottom panel). Together, these data reveal that the removal of defective cells by apoptosis is essential for the *C. elegans* germ line to recover following a breakdown in RNA splicing.

Functional gametes are generated from distal progenitors after MOG-7 recovery

What is the source of viable gametes that enables germline recovery upon restoring MOG-7 expression? We reasoned that

Fig. 5 Apoptosis is required for recovery from MOG-7 depletion. In all experiments in this figure, *mog-7::degron::gfp; sun-1p::TIR1::mRuby* hermaphrodites were used. **A** Experimental outline of MOG-7 depletion and recovery experiments. Early L4s were incubated on auxin plates for 18 h after which animals were transferred to plates without auxin (MOG-7::degron:::GFP was detected within 1 h of auxin removal; Supplementary Fig. S7) and brood size scored every 24 h. Control animals were either continually exposed to auxin (continual MOG-7 AID) or control (ethanol-treated) from the L4 stage. **B** Quantification of daily brood size of control (black line), continual MOG-7 AID (blue box) or recovering from 18 h MOG-7 AID (red line). Broods were scored on days 1–6 following removal of auxin. Data expressed as mean ± SD and statistical significance (control vs. 18 h MOG-7 AID) was assessed by multiple *t*-tests with Holm–Sidak correction. $n = 9$–10. **C**, **D** Fluorescence micrographs (**C**) and quantification (**D**) of germ cell apoptosis (SYTO-12 staining). SYTO-12-positive nuclei were counted at hours 6, 12, 18, 24, 30, and 36 following 18 h MOG-7 AID (auxin removal). Data expressed as mean ± SEM and statistical significance was assessed by one-way ANOVA. $n = 40$ per time-point. Scale bar = 20 µm. **E** Quantification of germ cell apoptosis (SYTO-12 staining) +/– *ced-3* RNAi. SYTO-12 positive nuclei were counted 18 h following removal of auxin. Data expressed as mean ± SEM and statistical significance was assessed by one-way ANOVA multiple comparison with Sidak correction. $n = 75$. **F** Quantification of germ cell apoptosis (SYTO-12 staining) in apoptotic pathway gene mutants—*lin-35(n745)*, *cep-1(rp165rp167)*, *egl-1(n1084n3082)*, and *ced-13(tm536)* compared to control animals. SYTO-12 positive nuclei were counted 18 h following removal of auxin. Data expressed as mean ± SEM and statistical significance was assessed by one-way ANOVA multiple comparison with Sidak correction. $n = 75$. **G** Quantification of total brood of exposed hermaphrodites +/– *ced-3* RNAi. Data expressed as mean ± SEM and statistical significance was assessed by unpaired *t*-test. $n = 9$–10. **H** Fluorescence micrographs of exposed hermaphrodites +/– *ced-3* RNAi. Germlines were extruded 48 h after auxin removal. Germ lines stained with DAPI to visualize DNA (white). Scale bar = 25 µm. Upper panel: pink dashed line = oocytes, blue dashed line = spermatheca, green dashed area = developing embryos. Lower panel: red lines = endomitotic nuclei/defective germ cells.

these gametes either originate from arrested/slow cycling germ cells in the PZ that re-enter the cell cycle or that meiotic germ cells can resolve the molecular and cellular deficits caused by MOG-7 depletion. To distinguish these scenarios, we used EdU to label germ cells generated in the PZ during MOG-7 depletion (in-auxin EdU) or after MOG-7 expression was restored (post-auxin EdU) (Fig. 6A). In-auxin EdU was applied 2 h after commencing auxin treatment to ensure that EdU-labeled germ cells are MOG-7 depleted (Fig. 6A).

After 16 h of in-auxin EdU labeling, most germ cells are EdU^+, confirming cell cycle progression occurs during MOG-7 depletion (Fig. 6B, 0 h time-point). Previously, we identified a cohort of arrested germ cells in MOG-7 depleted germ lines (Fig. 2H, J). We hypothesized that these germ cells may re-enter the cell cycle to replenish the germ line after restoring MOG-7 expression. Consistent with this, after removing auxin and EdU, we observed many distal EdU^- germ cells, suggesting that these cells re-entered the cell cycle after restoring MOG-7 expression (Fig. 6B, 12–24 h time-points). Germ cells that are labeled with EdU 24 h after auxin/EdU removal are mostly ectopic sperm/spermatocytes, oocytes, and germ cells with highly condensed proximal nuclei that are likely cleared by apoptosis (Fig. 6B, 24 h time-point). These EdU^+ cells could have been generated during MOG-7 depletion or while MOG-7 expression was being restored, but likely have irreparable splicing defects due to the extended loss of MOG-7.

In post-auxin EdU labeling, ectopic sperm/spermatocytes (Fig. 6C, blue line in 24 h time-point) and a small number of highly condensed proximal nuclei (Fig. 6C, red dashed box in 24 h time-point) are EdU^+, indicating that they were labeled after auxin removal. However, most of these highly condensed proximal nuclei are EdU^-, suggesting they were generated during MOG-7 depletion and exited the cell cycle prior to auxin removal (Fig. 6C, red dashed box in 24 h time-point). These data reveal that (1) germ cells entering meiosis during MOG-7 depletion are unable to functionally recover and are likely cleared by apoptosis, and (2) that the initial cohort of germ cells generated after restoring MOG-7 expression acquire the sperm fate. In support of this, ~60% of germlines are spermatogenic 24–36 h after auxin removal, with the oogenic program resuming after 48 h (Supplementary Fig. S9). Together, these data suggest that germline recovery requires the generation of new germ cells in the PZ. To independently verify this hypothesis, we used RNAi to knockdown expression of CDK-1, a cyclin-dependent kinase required for mitotic divisions [37]. We found that germline recovery from MOG-7 depletion requires CDK-1 function (Supplementary Fig. S10).

DISCUSSION

In this study, we identified a critical function for the previously uncharacterized protein MOG-7 in the *C. elegans* hermaphrodite germ line. We found that germline-specific loss of MOG-7 causes fully penetrant sterility. We observed multiple germ cell morphology and cell cycle defects in MOG-7 depleted germ lines that likely prevent the generation of viable gametes. Detection of in vivo MOG-7-interacting proteins identified multiple pre-mRNA splicing factors with known roles in spliceosome disassembly. To support the function of MOG-7 in pre-mRNA splicing, we found that MOG-7 is important for removal of introns from over 5000 protein-coding genes in the germ line. Despite being encumbered by extensive cellular and molecular deficits, hermaphrodites can become fertile within hours of restoring MOG-7 expression. As part of its recovery, the germ line undergoes a burst of apoptotic death, presumably to remove defective germ cells and to provide recycled cytoplasmic components for a newly generated germ cell cohort. Indeed, if apoptosis is inhibited MOG-7-recovered animals are sterile. We detected a slowing of the cell cycle and germ cell arrest in the distal germ line following long-term MOG-7 depletion. Collectively, these cells likely provide the source of fertile gametes once MOG-7 expression and correct pre-mRNA splicing is restored to the germ line. Together, these observations highlight the remarkable plasticity of the germ line and its ability to recover from extensive defects in fundamental cellular and molecular functions.

MOG-7 is orthologous to yeast and human splicing factors

In *S. cerevisiae*, the Nineteen complex-related proteins Ntr1 and Ntr2 are critical regulators of spliceosome disassembly [15, 17]. Ntr2 promotes the recruitment of Ntr1 to the ILS complex. Ntr1 then binds and activates Prp43 that induces spliceosome disassembly, where spliced introns are degraded and spliceosomal proteins recycled. The human genome does not encode a recognizable Ntr2 ortholog. However, the C2orf3 protein, which contains a GC-rich sequence DNA-binding factor (GCFC) domain, interacts with the human ortholog of Ntr1 (TFIP11), in addition to Prp43, and is involved in intron turnover [18]. The *mog-7* locus encodes two proteins related to Ntr2 (*S. cerevisiae*) and GCFC (human). MOG-7a contains both an Ntr2 and GCFC domain, whereas MOG-7b contains only the GCFC domain. Our experiments show that removal of both MOG-7 isoforms causes intron retention, germ cell defects and sterility. Furthermore, both MOG-7a and MOG-7b interact with the *C. elegans* spliceosome components we identified by MS. Our in vitro IP experiments showed that both the Ntr2 and GCFC domains of MOG-7 can interact with spliceosome proteins. In other organisms, the Ntr2

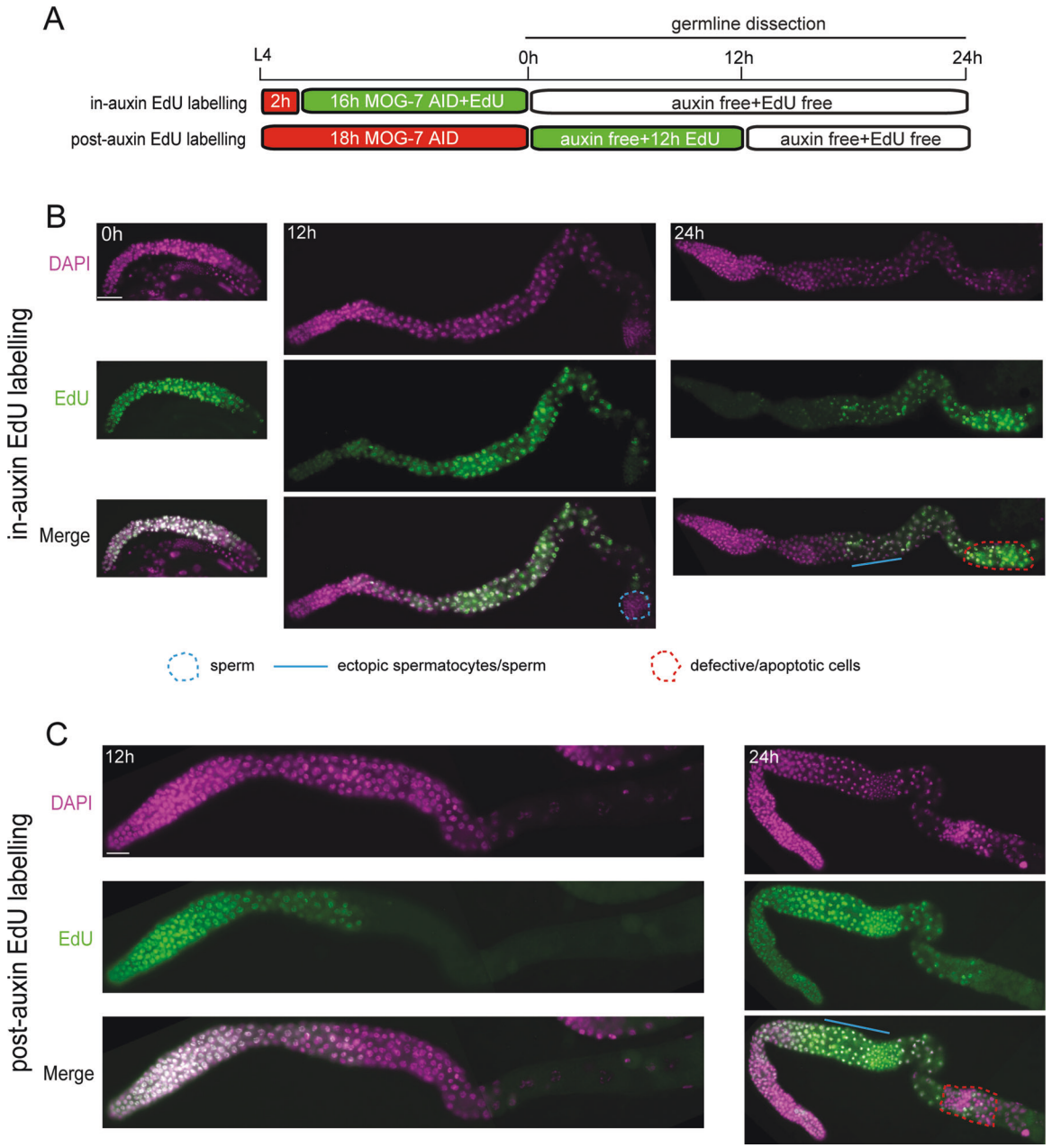

Fig. 6 New gametes are generated after MOG-7 is resupplied. A Experimental outline for S-phase labeling of adult germ cells following *mog-7* depletion and recovery. Early L4 *mog-7::degron::gfp; sun-1p::TIR1::mRuby* hermaphrodites were incubated as follows: in-auxin labeling (2 h auxin, 16 h auxin + EdU, 24 h auxin free and EdU free); post-auxin EdU labeling (18 h auxin, 12 h auxin free and 12 h EdU, 12 h auxin free and EdU free). Germ lines were extruded and analyzed at 0, 12, and 24 h following the 18 h of MOG-7 depletion in both labeling methods. **B**, **C** Fluorescence micrographs of germ lines exposed to in-auxin EdU labeling (**B**) and post-auxin EdU labeling (**C**). Germ lines stained with DAPI to visualize DNA (magenta) and labeled with EdU to detect replicated DNA (green). Ectopic spermatocytes/sperm = blue line/dashed line. Defective/apoptotic cells = red dashed area. Scale bar = 20 µm.

and GCFC domains are present in distinct proteins [15, 18]. Whether the MOG-7a (Ntr2 and GCFC) and MOG-7b (GCFC only) isoforms perform cell-specific or spliceosome complex-specific roles is unknown and is an interesting avenue of future investigation.

Loss of MOG-7 rapidly causes intron retention

Spliceosomes form on each newly synthesized intron before disassembling for the next round of splicing [38]. In a highly ordered process, spliceosome sub-complexes sequentially associate with each intron in a reversible manner [39]. Hence, an interruption in spliceosome protein disassembly inhibits the splicing of subsequent transcripts. We found that MOG-7 directly interacts with multiple splicing factors involved with spliceosome disassembly and observed extensive intron retention within 1 h of depleting the MOG-7 protein. Such rapid retention of introns suggests that the splicing process is highly sensitive to MOG-7 removal and that perhaps introns are retained even as MOG-7 protein levels start to reduce following auxin treatment. We have shown that restoring MOG-7 expression following long-term MOG-7 depletion enables animals to become fertile. Whether restoring MOG-7 expression enables spliceosomes to reform and initiate splicing on incorrectly spliced transcripts or whether new transcription is required for recovery is unknown. The requirement

for apoptosis in the recovery process (see below) indicates that many germ cells, and their defective transcripts, need to be removed to enable the generation of functional gametes. However, there may be a cohort of germ cells that can functionally recover from the splicing defects.

MOG-7 depletion affects germ cell morphology and cell cycle progression

A previous study showed that starving adult hermaphrodites causes cell-cycle arrest where germ cells stop dividing and become quiescent [40]. These germ cells exhibit a slowing of S-phase and arrest in G2 of the cell cycle. Upon re-feeding these quiescent cells rapidly re-enter M-phase and produce viable progeny [40]. Our analysis of the germ line following MOG-7 depletion revealed multiple defects in germ cell nuclear morphology, clustering of germ cells, and areas of the germ line devoid of germ cells. In addition, the PZs of MOG-7 depleted animals have a reduced number of germ cells in M-phase and S-phase of the cell cycle. These findings suggest a slowing of the germ cell cycle in the PZ in response to the splicing defects. Examination of germ lines following long-term MOG-7 depletion also revealed a number of arrested germ cells (Fig. 2) that are likely a source of new gametes.

Apoptotic disposal of germ cells enables recovery from MOG-7 depletion

In the hermaphrodite germ line, both physiological and stress-induced germ cell death require induction of the core apoptotic caspase CED-3 [4, 6]. When we resupplied MOG-7 following MOG-7 depletion, the germ line exhibited a burst of apoptosis that was dependent on CED-3. Initiation of apoptosis did not occur until 18 h after MOG-7 expression was restored. This delay may be caused by the defective splicing of genes required for apoptosis in MOG-7-depleted germ lines, such that these mis-spliced transcripts need to be resolved and/or new transcription activated prior to initiation of apoptosis. In support of this premise, transcripts of the core apoptotic pathway genes (*ced-3*, *ced-4*, *ced-9*) contain retained introns within 1 h of MOG-7 depletion (Supplementary Table S3). We showed that *ced-3* knockdown caused sterility in MOG-7-recovered but in not control animals. Indeed, the proximal end of MOG-7-recovered *ced-3* knockdown germ lines is replete with aberrant germ cells. This confirms the importance of removing defective germ cells by apoptosis for germline recovery after resupplying MOG-7 expression. Parallel pathways act upstream of CED-3 to control physiological (LIN-35/Retinoblastoma) and stress-induced germ cell death (CEP-1/p53, EGL-1/BH3-only, and CED-13/BH3-only) [33–35]. We found that LIN-35, CEP-1, and EGL-1 but not CED-13 are partially required for apoptotic induction in MOG-7 AID recovered germlines. This suggests that defective splicing in MOG-7 depleted germlines may not only cause extensive gene expression changes, but possibly also DNA and cellular damage that trigger apoptosis. The role of each cell death pathway in this context may therefore be dependent on the nature of the germ cell defect and/or the stage of the germ cell cycle at which splicing collapse occurs.

Regulation of sperm/oocyte cell fate

Multiple studies have previously revealed that downregulation of splicing factors causes inappropriate masculinization of the germ line (Mog phenotype) [8, 9, 12, 13, 21, 41, 42]. Indeed, *F43G9.12/mog-7* RNAi knockdown was previously shown to cause synthetic germline masculinization and lethality in mutants for the PUF domain RNA-binding proteins FBF-1 and FBF-2 [9]. These FBF proteins repress genes that promote differentiation, meiotic processes, and genes associated with spermatogenesis [43–45]. This study also found that RNAi knockdown of *F43G9.12/mog-7* alone resulted in a low penetrant Mog phenotype [9]. We took advantage of the AID system to completely remove F43G9.12/MOG-7 protein at different developmental time-points. We revealed that removing MOG-7 at the L3 larval stage caused masculinization of most germ lines, whereas removing MOG-7 from the L4 stage resulted in mostly oogenic germ lines. This suggests the importance of splicing regulation prior to/during the sperm-oocyte switch.

When examining germline behavior during recovery from MOG-7 depletion, we identified an interesting switch in germ line sexual fates. As mentioned previously, continuous MOG-7 AID from L4 resulted in mostly oogenic germline development. Indeed, when we depleted MOG-7 from early L4 to the first day of adulthood, we initially observed oogenic germ lines. However, 24 and 36 h after restoring MOG-7 expression the germ lines were spermatogenic, and then reverted to oogenesis 12 h later. The initial oogenic phase during MOG-7 recovery likely enables the apoptotic program (oogenic-specific) to remove defective germ cells [4]. After the defective germ cells are removed, the germ line then re-enters a new phase of spermatogenesis prior to generating oocytes. These findings highlight the plasticity of the germ line and perhaps the sensitivity of cells at different stages of the cell cycle and differentiation process to a disruption in splicing.

Together, this study reveals the ability of the *C. elegans* germ line to recover functionality following a breakdown in pre-mRNA splicing. Removal of the MOG-7 splicing factor induces multiple defects in germ cell morphology and behavior throughout the germ line that leads to sterility. After restoring MOG-7 expression in adults, the germ line initiates apoptotic clearance of defective germ cells and re-initiation of germ cell proliferation.

EXPERIMENTAL PROCEDURES

Contact for reagent and resource sharing

Strains used in this study will be deposited at the *Caenorhabditis* Genetics Center and will be available upon request. Further information and requests for resources and reagents should be directed to and will be fulfilled by the Lead Contact Roger Pocock (roger.pocock@monash.edu).

Experimental models and subject details

Caenorhabditis elegans. *C. elegans* strains were cultured on Nematode Growth Medium (NGM) plates and fed with OP50 *Escherichia coli* bacteria at 20 °C, unless otherwise stated. All strains used in this study are listed in Supplementary Table S4. Experiments were performed in triplicates and the number of animals analyzed is annotated in each figure and legend where appropriate.

Mammalian cells. For co-immunoprecipitation experiments, COS-7 cells were cultured in Dulbecco's Modified Eagle Medium (containing 4500 mg/L d-glucose, 584 mg/L L-glutamine, 110 mg/L sodium pyruvate) (Thermo Fisher) containing 1% penicillin and streptomycin (Invitrogen), 5 µM L-glutamine (Life Technologies), and 5% fetal bovine serum (Thermo Fisher).

Endogenous tagging of MOG-7 with degron::GFP using CRISPR-Cas9

A C-terminal MOG-7::degron::GFP knock-in strain was generated using CRISPR/Cas9-triggered homologous recombination [22]. The crRNA used to target *mog-7* was designed and ordered using the online tool provided by https://sg.idtdna.com (Supplementary Table S6). Asymmetric-hybrid donor repair templates were generated by PCR using ultramer primers (Supplementary Table S6). The following mix was then injected into wild-type animals: 4 µg repair template, 5 µg Cas9 protein, 2 µg universal tracrRNA, 1.1 µg crRNA, *myo-2::mCherry* plasmid (4 ng/µL). Individual F1 progeny of injected wild-type worms were isolated and F2 progeny screened for *degron::gfp* knock-in by PCR. After confirmation of insertion by Sanger sequencing, the *degron::gfp*

knock-in was outcrossed three times prior to analysis. MOG-7::degron::GFP was imaged using a Zeiss Axiocam 40x objective.

Generating *cep-1* STOP-IN mutations using CRISPR-Cas9

STOP-IN mutations of *cep-1* were generated by inserting 43-nucleotide knock-in cassettes (STOP-IN) into the first exons of both the long and short *cep-1* isoforms using CRISPR/Cas9 gene editing [36]. The crRNAs used to target *cep-1* were designed and ordered using the online tool provided by https://sg.idtdna.com (Supplementary Table S6). Repair templates were ordered from IDT (Supplementary Table S6). To insert the STOP-IN cassette into the first exon of the *cep-1* short isoform, the following mix was injected into *mog-7::degron::gfp; sun-1p::TIR1* animals: 2.2 µg repair template, 5 µg Cas9 protein, 2 µg universal tracrRNA, 1.1 µg crRNA, 4 ng/µL *myo-2::mCherry* plasmid. After obtaining the correct *cep-1* short knock-in, the STOP-IN cassette was inserted in the first exon of the *cep-1* long isoform using *cep-1* long crRNA and repair template with the same injection strategy as above. Individual F1 progeny of injected animals was isolated and F2 progeny screened for each STOP-IN knock-in by PCR. After confirmation of insertion by Sanger sequencing, the knock-in strain was outcrossed once prior to analysis.

RNA interference experiments

HT115(DE3) *E. coli* bacteria expressing RNAi plasmids for specific genes or empty vector (L4440) were grown in Luria Broth (LB) + Ampicillin (50 µg/mL) at 37 °C for 16 h. Saturated cultures of RNAi bacteria were plated on RNAi plates and allowed to dry for 24 h. Hermaphrodite larvae were placed on the RNAi plates and incubated for various periods depending on the experiment (described in each figure legend).

Auxin-inducible degradation (AID) plates

NGM plates were supplemented with 0.1 or 1 mM Auxin (indole-3-acetic acid, Alfa Aesar, ALFA10556) from a stock of 400 mM dissolved in ethanol. NGM plates supplemented with ethanol were used as a control.

Brood size analysis

Ten L4 hermaphrodites were picked onto individual NGM plates seeded with OP50 bacteria. Worms were allowed to lay eggs for 24 h and then the mothers were individually moved to new plates. After a further 24 h, embryos were analyzed for hatching. This process was repeated for 6 days. The number of larvae and embryos were counted each day and summed as the total brood size.

Transfection of COS-7 cells

A total of 60,000 cells were transferred into each well of a 24-well plate. Plasmid transfection was performed when cells were approximately 70% confluent. In each well, 0.25 µL of plasmid was mixed with 70 µL Opti-MEM®, and 2.5 µL lipofectamine was mixed with 70 µL Opti-MEM®. After incubating at room temperature for 5 min, the two mixtures were combined and incubated at room temperature for 20 min. The 140 µL transfection complexes were applied to each well. After incubating in 37 °C for 3 h, 1 mL of fresh media was added to each well and cells were harvested 1 day after the transfection.

Cell lysis and co-immunoprecipitation

Each cell culture well was washed three times with cold 1× phosphate buffered saline (PBS) buffer before 100 µL cell lysis buffer (containing 50 mM Tris pH 7.6, 150 mM NaCl, 1% TX-100, cOmplete™ EDTA-free Protease Inhibitor Cocktail) was added. Cells were scraped off the bottom of the plate and sonicated (10 s on, 20 s off, three cycles) before being centrifuged at the highest speed for 10 min. Then, 20 µL of the supernatant was extracted as the input.

One microliter Mouse anti-V5 antibody was added to every 10 µL Dynabeads™ protein G (Thermo Fisher Scientific) (2.5 µL per sample) and left to incubate overnight to facilitate binding before use. Crosslinking was performed by incubating the antibody-coupled Dynabeads™ in 250 µL 5 mM Pierce BS3 Crosslinker (in PBS buffer) rotating for 30 min at room temperature. The crosslinking reaction was then quenched by adding 12.5 µL 1 M Tris HCl (pH 8). After washing thrice with 1× PBS buffer, the cross-linked Ab-Dynabeads™ were added into the supernatant of cell lysates for IP. After a 2 h incubation, the Dynabeads™ were isolated using a magnet, and washed thrice with cell lysis buffer.

Western blotting

COS-7 samples. After mixing with 1xBolt™ LDS sample buffer (Invitrogen™) and 1xBolt™ Sample reducing Agent (Invitrogen™), the input sample and post-immunoprecipitation Dynabeads™ were boiled at 95 °C for 5 min. A total of 10% resolving gels were used to separate proteins, except for samples containing FLAG-PRP-8 (276 kD), in which case 6% resolving gels were used. SDS-PAGE was performed in a Mini-PROTEAN Tetra Vertical Electrophoresis Cell (Bio-Rad) filled with 1× SDS-PAGE Running buffer (10× SDS-PAGE Running buffer: 30 g of Tris base, 144 g of glycine, and 10 g of SDS in 1000 mL of H_2O). Voltage of 60 and 120 V were respectively used for stacking and protein separation, respectively. After separation on an SDS-PAGE gel, proteins were transferred to the PVDF membrane by using iBlot™ 2 Transfer Stacks (Thermo Fisher Scientific) and iBlot™ 2 Gel Transfer Device (Thermo Fisher Scientific) according to the manufacturer's instructions. After blotting, the PVDF membrane was blocked through incubation in 5% w/v bovine serum albumin (in 1× PBS) at room temperature for 30 min. Subsequently, the membrane was incubated in primary antibody at 4 °C overnight, followed by an incubation with secondary antibodies at room temperature for 1.5 h. Primary antibodies (Mouse anti-FLAG/DYKDDDDK tag antibody (2368, Cell Signaling), Mouse anti-V5 tag antibody (SV5-Pk1, Bio-Rad)) and secondary antibodies (Goat anti-Mouse IgG (H+L) secondary antibody, HRP conjugate (32430, Thermo Fisher Scientific)) were diluted (1:1000) in 1% w/v bovine serum albumin (in 1× PBS). Then, 1× PBS (containing 0.1% Tween-20) was used to wash the membrane after each antibody incubation. Proteins were detected using the EZ-ECL Chemiluminescence Detection Kit for HRP (Biological Industries) and ChemiDoc XRS+ Gel Documentation System (Bio-Rad Laboratories). Images were taken using the ImageLab™ software (Bio-Rad).

C. elegans samples. Transgenic worms expressing degron::GFP-tagged MOG-7 were grown on NGM plates coated with OP50 bacteria. A packed volume of 1 mL of mixed-stage worms and embryos was collected by washing with M9 buffer. Worms were washed three times with M9 buffer, pelleted by centrifugation and 3 mL of lysis buffer (50 mM Tris pH 7.4, 150 mM NaCl, 2% triton X-100, 0.1% SDS, 1× protease inhibitor cocktail) was added. Worms were disrupted using a mortar and pestle, then sonicated using Bioruptor® (Diagenode) at high amplitude (4 °C; 30 s on and 20 s off) for 10–15 cycles. After centrifuging at 3000 rpm for 5 min, the supernatant was collected and GFP-Trap® (Chromotek) was used to precipitate MOG-7::degron::GFP. Samples were cooled to room temperature and run on a 10% polyacrylamide gel. The gel was blotted to a PVDF membrane using the iBlot semi-dry blot system (Thermo Fisher). After blocking with 5% BSA in PBS for 1 h, the PVDF membranes were incubated with anti-GFP antibody (Roche) in 1% BSA in PBS-tween (0.1%) for 16 h at 4 °C. The membrane was then washed three times with PBS-tween and incubated with horseradish peroxidase-conjugated secondary antibodies in 1% BSA in PBS-tween for 1 h at 22 °C. The membrane was washed five times with PBS-tween and incubated with ECL reagents (Thermo Fisher) for 2 min at room temperature. The membrane was

exposed using Biorad ChemiDoc XRS+ and images taken using a CCD camera and Image Lab 6.0.1 software.

Mass spectrometry

Mixed-stage worms containing mostly 1-day-old adults, L1s and embryos were harvested for MS analysis. Approximately, 400,000 adults/per sample were required for robust MOG-7::degron::GFP pulldown. Three genotypes were analyzed in each MS experiment: *sun-1p::TIR1; mog-7::degron::gfp*, *evIs111* (GFP-only control), wild-type (no fluorophore control). Harvested worms were washed with M9 buffer (five times), before adding three times dry worm volume of RIPA buffer. After grinding and sonicating (30 s on, 30 s off, 30 cycles), each sample was incubated with a mixture of 10 µL IgG conjugated magnetic beads (Cell Signaling) and 10 µL Dynabeads™ for 1 h to preclear. After removing the IgG conjugated magnetic beads, each sample was incubated with 10 µL GFP-Trap® (Chromotek) at 4 °C overnight for IP, and a *sun-1p::TIR1; mog-7::degron::gfp* sample was incubated with 10 µL IgG conjugated magnetic beads (Cell Signaling) as a control.

Magnetic beads were collected using a magnet and washed with buffers in the following order: wash buffer 1 (RIPA buffer—50 mM Tris pH 7.6, 150 mM NaCl, 1% TX-100, 0.1% SDS), wash buffer 2 (50 mM Tris pH 8.0, 150 mM NaCl), wash buffer 3 (50 mM Tris pH 8.0, 450 mM NaCl), and wash buffer 4 (50 mM Tris pH 8.0). Then, beads were then incubated in 150 µL 0.2 M glycine (pH 2.5) for 5 min to elute the protein. The elution was repeated thrice, and the combined 450 µL of eluted samples were neutralized with ~80 µL 1 M Tris/HCl pH 8.0.

MS analysis was performed by Monash Biomedical Proteomics Facility. The Nano LC system used in this study was the Dionex Ultimate 3000 RSLCnano, the Mass spectrometer used was the QExactive Plus 2 (Thermo Scientific), the analytical column used was the Acclaim PepMap RSLC (75 µm × 50 cm, nanoViper, C18, 2 µm, 100 Å; Thermo Scientific), and the Trap column used was the Acclaim PepMap 100 (100 µm × 2 cm, nanoViper, C18, 5 µm, 100 Å; Thermo Scientific). The search engine Byonic (ProteinMetrics) was used for data analysis.

Molecular cloning

For mammalian expression, the following plasmids were used to insert *C. elegans* cDNA sequences: pcDNA3.1(zeo) and p3XFLAG-CMV-10.

mog-7acDNA::V5 *tag*. The *mog-7a cDNA::V5* mammalian expression construct was generated by cloning the 2430 bp *mog-7a* cDNA with HindIII into the pcDNA3.1(zeo) expression vector.

mog-7bcDNA::V5 *tag*. The *mog-7b cDNA::V5* mammalian expression construct was generated by cloning the 930 bp *mog-7b cDNA* with HindIII into the pcDNA3.1(zeo) expression vector.

eftu-2cDNA::FLAG *tag*. The *eftu-2cDNA::FLAG* mammalian expression construct was generated by cloning the 2925 bp *eftu-2* cDNA with NheI-HindIII into the p3XFLAG-CMV-10 expression vector.

Y94H6A.3cDNA::FLAG *tag*. The *Y94H6A.3cDNA::FLAG* mammalian expression construct was generated by cloning the 561 bp *Y94H6A.3* cDNA with KpnI into the p3XFLAG-CMV-10 expression vector.

stip-1cDNA::FLAG *tag*. The *stip-1cDNA::FLAG* mammalian expression construct was generated by cloning the 2493 bp *stip-1* cDNA with XbaI into the p3XFLAG-CMV-10 expression vector.

prp-8cDNA::FLAG *tag*. The *prp-8cDNA::FLAG* mammalian expression construct was generated by cloning the 6990 bp *prp-8* cDNA with XbaI into the p3XFLAG-CMV-10 expression vector.

skp-1cDNA::FLAG *tag*. The *skp-1cDNA::FLAG* mammalian expression construct was generated by cloning the 1608 bp skp-1 cDNA with XbaI into the p3XFLAG-CMV-10 expression vector.

prp-19cDNA::FLAG *tag*. The *prp-19cDNA::FLAG* mammalian expression construct was generated by cloning the 1930 bp *prp-19* cDNA with XbaI into the p3XFLAG-CMV-10 expression vector.

Germline analysis

Germline analysis was performed as previously reported [46]. L4 hermaphrodites were picked to OP50 plates and incubated for 16 h at 20 °C to reach the young adult stage. Germ lines were extruded from sedated worms and fixed on a poly-L-lysine coated slides using ice cold methanol for 1 min and then in 3.7% paraformaldehyde for 25 min. Fixed germ lines were washed three times in PBS (pH 7.4) and blocked using 30% normal goat serum before incubating with primary antibodies overnight at 4 °C. After incubation, germ lines were washed three times with PBS containing 1% Tween-20 (PBST) and incubated with fluorophore-conjugated secondary antibodies and DAPI for 1 h at 25 °C. After staining, germ lines were washed three times with PBST. Slides were mounted by applying a drop of Fluoroshield mounting media (Sigma) on the germ lines followed by a coverslip. Stained germ lines were analyzed using the Zeiss Axiocam 40× objective or the Leica SP5 63× objective. Germ cell number and 3D modeling were performed using Imaris 9.5. The diameter of DAPI-stained nuclei in the mitotic region was defined as 2.5 µm and a three-dimensional model was created to enable counting of nuclei. To quantify the number of cells in active mitosis, extruded germ lines were stained with an anti-pH3 antibody and pH3-positive nuclei counted.

EdU labeling was performed as in previous studies [25, 47]. NGM agar plates (-peptone, 60 µg/mL carbenicillin) were seeded with concentrated *E. coli* MG1693 that was grown in *E. coli* M9 minimal media (3 g/L KH_2PO_4, 6 g/L Na_2HPO_4, 0.5 g/L NaCl, 1 g/L NH_4Cl, 2 mM $MgSO_4$, 0.1 mM $CaCl_2$, 0.4% glucose, 1.25 µg/mL thiamin) supplemented with 0.5 µM thymidine and 20 µM EdU for 24 h. Auxin and ethanol were added to NGM agar accordingly. Following EdU feeding and germline isolation, fixation was performed as above. The Click reaction was performed according to the manufacturer instructions (Invitrogen™, C10337), and DNA was stained by DAPI. Stained germ lines were analyzed using the Nikon C1 Confocal Microscope 60× objective.

Analysis of germline apoptosis

Synchronized 1-day-old adults and OP50 bacteria were washed with M9 buffer, and a final concentration of 50 µM SYTO-12 (Thermo Scientific™) added to the worm/bacteria mixture. After incubation at 25 °C for 5 h, worms were transferred to a fresh seeded plate for 1 h to allow the stained bacteria to be purged from the gut to reduce background fluorescence. Worms were then mounted on agarose pads for the scoring of apoptosis nuclei which emit green fluorescence.

Fluorescence microscopy of *C. elegans*

Animals were anesthetized with 20 mM NaN_3 on 5% agarose pads, and images were obtained with an Axio Imager M2 fluorescence microscope and Zen software (Zeiss).

RNA sequencing

On entering adulthood, a synchronized population of *mog-7::degron::GFP; sun-1p::TIR1* hermaphrodites was evenly divided into three groups (~1000 animals per sample), with two groups incubated either on 1 mM auxin or ethanol (control) for 2 h. After 1 h, the remaining group was incubated on 1 mM auxin for 1 h. Six replicates of each sample were collected for RNA extraction and sequencing.

Bioinformatics methods

Raw reads were first trimmed for adapter content and low-quality base-calls using Trimmomatic [48] in palindrome mode, using a sliding window of 5 nt with quality threshold 15, removing any reads <40 nt after the trimming. Cutadapt was then used to remove reads with SL-1 and SL-2 spliced-leader sequences, followed by a first-pass mapping of reads to the WBCel235.99 genome using STAR [49], with conservative parameters for novel splice sites (alignSJDBoverhangMin 10). The splice junction files from this first-pass mapping were used with more liberal settings in STAR (alignSJDBoverhangMin 4) in a second-pass alignment of the reads. Duplicate alignments were marked with Picard MarkDuplicates and alignments sorted with Samtools [50].

These unfiltered alignments were used to analyze retained introns. A custom annotation was produced that only contained intronic sequences from the WBCel235.99 annotation as counting-bins, and featureCounts [51] was then used to count any read ovelapping an intron by more than 3 nt. The EdgeR quasi-likelihood method [52] was used to identify introns that were differentially represented in the 1 h auxin-treated samples. Only introns with at least five reads in one of the samples and at least three samples with counts-per-million-intronic-reads above 0.5 were included for analysis. Because the auxin-treated samples were so skewed toward intronic sequences, and only intronic alignments were counted in each library, a custom library-size normalization was used whereby the log-fold-change (treated–untreated) was modeled as two normal distributions (using the function normalMixEM in the R package mixtools) and only the introns in the lower fold-change population (about 9000 introns) were used to generate library normalization factors. 17,647 introns in 5014 genes were identified as differentially present in 1 h treated samples, at a false discovery rate of 0.001. Apart from analysis of specific introns, the unfiltered alignments were also used to assess the genome-wide increase in non-exonic mRNA in the treated animals (Fig. 4 and Supplementary Fig. S5).

Strictly exonic versions of the read alignments were generated in order to assess differences in gene expression and canonical splice site selection between auxin-treated and control samples, without interference from the significant amounts of non-canonical transcript/intronic/intergenic RNA found in the treated worms. Custom scripts were used to remove reads if an alignment overlaps any non-exonic region by more than 3 nt, according to the WBCel235.99 annotation. For calling DEGs, featureCounts [51] was used to count read alignments per gene and Limma Voom [53] in Degust was used to perform the statistical analysis.

RT-PCR assays

Total RNA was isolated using the RNeasy Mini Kit (QIAGEN 74104), according to the manufacturer's instructions. In all, 500 ng of RNA was reverse-transcribed to cDNA using 0.5 mg/mL oligodT primers and the ImProm-II Reverse Transcription System (A3800) followed. cDNA was diluted to 1:5 in RNAse-free water. RT-PCR amplicons were run on a standard DNA electrophoresis gel.

Quantification and statistical analysis

All experiments were performed in three independent replicates and the experimenter was blinded to genotype. Statistical analysis was performed in GraphPad Prism 7 using one-way analysis of variance for comparison followed by Dunnett's multiple comparison test where applicable. Welch's *t*-test was performed if the comparison was for two conditions. Values are expressed as mean ± SEM. Differences with a p value < 0.05 were considered significant.

DATA AVAILABILITY

Data are available in the main text or the Supplementary materials. Sequencing data are available under NCBI accession number GSE162055.

REFERENCES

1. Gao DL, Kimble J. Apx-1 can substitute for its homolog Lag-2 to direct cell-interactions throughout *Caenorhabditis-elegans* development. Proc Natl Acad Sci USA. 1995;92:9839–42.
2. Henderson ST, Gao D, Lambie EJ, Kimble J. Lag-2 may encode a signaling ligand for the Glp-1 and Lin-12 receptors of *C-elegans*. Development. 1994;120:2913–24.
3. Kulkarni M, Shakes DC, Guevel K, Smith HE. SPE-44 implements sperm cell fate. PLoS Genet. 2012;8:e1002678.
4. Gumienny TL, Lambie E, Hartwieg E, Horvitz HR, Hengartner MO. Genetic control of programmed cell death in the *Caenorhabditis elegans* hermaphrodite germline. Development. 1999;126:1011–22.
5. Aballay A, Ausubel FM. Programmed cell death mediated by ced-3 and ced-4 protects *Caenorhabditis elegans* from *Salmonella typhimurium*-mediated killing. Proc Natl Acad Sci USA. 2001;98:2735–9.
6. Gartner A, Milstein S, Ahmed S, Hodgkin J, Hengartner MO. A conserved checkpoint pathway mediates DNA damage-induced apoptosis and cell cycle arrest in *C. elegans*. Mol Cell. 2000;5:435–43.
7. Salinas LS, Maldonado E, Navarro RE. Stress-induced germ cell apoptosis by a p53 independent pathway in *Caenorhabditis elegans*. Cell Death Differ. 2006;13:2129–39.
8. Kerins JA, Hanazawa M, Dorsett M, Schedl T. PRP-17 and the pre-mRNA splicing pathway are preferentially required for the proliferation versus meiotic development decision and germline sex determination in *Caenorhabditis elegans*. Dev Dyn. 2010;239:1555–72.
9. Novak P, Wang X, Ellenbecker M, Feilzer S, Voronina E. Splicing machinery facilitates post-transcriptional regulation by FBFs and other RNA-binding proteins in *Caenorhabditis elegans* germline. G3 (Bethesda). 2015;5:2051–9.
10. Hoskins AA, Moore MJ. The spliceosome: a flexible, reversible macromolecular machine. Trends Biochem Sci. 2012;37:179–88.
11. Wahl MC, Will CL, Luhrmann R. The spliceosome: design principles of a dynamic RNP machine. Cell. 2009;136:701–18.
12. Graham PL, Kimble J. The Mog-1 gene is required for the switch from spermatogenesis to oogenesis in *Caenorhabditis-elegans*. Genetics. 1993;133:919–31.
13. Graham PL, Schedl T, Kimble J. More Mog genes that influence the switch from spermatogenesis to oogenesis in the hermaphrodite germ-line of *Caenorhabditis-elegans*. Developmental Genet. 1993;14:471–84.
14. Zanetti S, Puoti A. Sex determination in the *Caenorhabditis elegans* germline. Adv Exp Med Biol. 2013;757:41–69.
15. Tsai RT, Fu RH, Yeh FL, Tseng CK, Lin YC, Huang YH, et al. Spliceosome disassembly catalyzed by Prp43 and its associated components Ntr1 and Ntr2. Genes Dev. 2005;19:2991–3003.
16. Fourmann JB, Tauchert MJ, Ficner R, Fabrizio P, Luhrmann R. Regulation of Prp43-mediated disassembly of spliceosomes by its cofactors Ntr1 and Ntr2. Nucleic Acids Res. 2017;45:4068–80.
17. Tsai RT, Tseng CK, Lee PJ, Chen HC, Fu RH, Chang KJ, et al. Dynamic interactions of Ntr1-Ntr2 with Prp43 and with U5 govern the recruitment of Prp43 to mediate spliceosome disassembly. Mol Cell Biol. 2007;27:8027–37.
18. Yoshimoto R, Okawa K, Yoshida M, Ohno M, Kataoka N. Identification of a novel component C2ORF3 in the lariat-intron complex: lack of C2ORF3 interferes with pre-mRNA splicing via intron turnover pathway. Genes Cells. 2014;19:78–87.
19. Konishi T, Uodome N, Sugimoto A. The *Caenorhabditis elegans* DDX-23, a homolog of yeast splicing factor PRP28, is required for the sperm-oocyte switch and differentiation of various cell types. Dev Dyn. 2008;237:2367–77.
20. Tsukamoto T, Gearhart MD, Kim S, Mekonnen G, Spike CA, Greenstein D. Insights into the involvement of spliceosomal mutations in myelodysplastic disorders from analysis of SACY-1/DDX41 in *Caenorhabditis elegans*. Genetics. 2020;214:869–93.
21. Zanetti S, Meola M, Bochud A, Puoti A. Role of the *C. elegans* U2 snRNP protein MOG-2 in sex determination, meiosis, and splice site selection. Dev Biol. 2011;354:232–41.
22. Dokshin GA, Ghanta KS, Piscopo KM, Mello CC. Robust genome editing with short single-stranded and long, partially single-stranded DNA donors in *Caenorhabditis elegans*. Genetics. 2018;210:781–7.
23. Zhang LY, Ward JD, Cheng Z, Dernburg AF. The auxin-inducible degradation (AID) system enables versatile conditional protein depletion in *C-elegans*. Development. 2015;142:4374–84.
24. Barton MK, Kimble J. Fog-1, a regulatory gene required for specification of spermatogenesis in the germ line of *Caenorhabditis-Elegans*. Genetics. 1990;125:29–39.
25. Crittenden SL, Seidel HS, Kimble J. Analysis of the *C. elegans* germline stem cell pool. Methods Mol Biol. 2017;1463:1–33.
26. Dernburg AF, McDonald K, Moulder G, Barstead R, Dresser M, Villeneuve AM. Meiotic recombination in *C. elegans* initiates by a conserved mechanism and is dispensable for homologous chromosome synapsis. Cell. 1998;94:387–98.

27. Cinquin O, Crittenden SL, Morgan DE, Kimble J. Progression from a stem cell-like state to early differentiation in the *C. elegans* germ line. Proc Natl Acad Sci USA. 2010;107:2048–53.
28. Wan R, Yan C, Bai R, Lei J, Shi Y. Structure of an intron lariat spliceosome from *Saccharomyces cerevisiae*. Cell. 2017;171:120–32.e112.
29. Fabrizio P, Dannenberg J, Dube P, Kastner B, Stark H, Urlaub H, et al. The evolutionarily conserved core design of the catalytic activation step of the yeast spliceosome. Mol Cell. 2009;36:593–608.
30. Kelly WG, Schaner CE, Dernburg AF, Lee MH, Kim SK, Villeneuve AM, et al. X-chromosome silencing in the germline of *C. elegans*. Development. 2002;129:479–92.
31. Jaramillo-Lambert A, Ellefson M, Villeneuve AM, Engebrecht J. Differential timing of S phases, X chromosome replication, and meiotic prophase in the *C-elegans* germ line. Developmental Biol. 2007;308:206–21.
32. Angelo G, Van, Gilst MR. Starvation protects germline stem cells and extends reproductive longevity in *C. elegans*. Science. 2009;326:954–8.
33. Schertel C, Conradt B. *C. elegans* orthologs of components of the RB tumor suppressor complex have distinct pro-apoptotic functions. Development. 2007;134:3691–701.
34. Schumacher B, Schertel C, Wittenburg N, Tuck S, Mitani S, Gartner A, et al. *C. elegans* ced-13 can promote apoptosis and is induced in response to DNA damage. Cell Death Differ. 2005;12:153–61.
35. Ye AL, Ragle JM, Conradt B, Bhalla N. Differential regulation of germline apoptosis in response to meiotic checkpoint activation. Genetics. 2014;198:995–1000.
36. Wang H, Park H, Liu J, Sternberg PW. An efficient genome editing strategy to generate putative null mutants in *Caenorhabditis elegans* using CRISPR/Cas9. G3 (Bethesda). 2018;8:3607–16.
37. Boxem M, Srinivasan DG, van den Heuvel S. The *Caenorhabditis elegans* gene ncc-1 encodes a cdc2-related kinase required for M phase in meiotic and mitotic cell divisions, but not for S phase. Development. 1999;126:2227–39.
38. Staley JP, Guthrie C. Mechanical devices of the spliceosome: motors, clocks, springs, and things. Cell. 1998;92:315–26.
39. Hoskins AA, Friedman LJ, Gallagher SS, Crawford DJ, Anderson EG, Wombacher R, et al. Ordered and dynamic assembly of single spliceosomes. Science. 2011;331:1289–95.
40. Seidel HS, Kimble J. Cell-cycle quiescence maintains *Caenorhabditis elegans* germline stem cells independent of GLP-1/Notch. Elife. 2015;4:e10832.
41. Puoti A, Kimble J. The *Caenorhabditis elegans* sex determination gene mog-1 encodes a member of the DEAH-box protein family. Mol Cell Biol. 1999;19:2189–97.
42. Puoti A, Kimble J. The hermaphrodite sperm/oocyte switch requires the *Caenorhabditis elegans* homologs of PRP2 and PRP22. Proc Natl Acad Sci USA. 2000;97:3276–81.
43. Crittenden SL, Bernstein DS, Bachorik JL, Thompson BE, Gallegos M, Petcherski AG, et al. A conserved RNA-binding protein controls germline stem cells in *Caenorhabditis elegans*. Nature. 2002;417:660–3.
44. Merritt C, Seydoux G. The Puf RNA-binding proteins FBF-1 and FBF-2 inhibit the expression of synaptonemal complex proteins in germline stem cells. Development. 2010;137:1787–98.
45. Thompson BE, Bernstein DS, Bachorik JL, Petcherski AG, Wickens M, Kimble J. Dose-dependent control of proliferation and sperm specification by FOG-1/CPEB. Development. 2005;132:3471–81.
46. Gopal S, Boag P, Pocock R. Automated three-dimensional reconstruction of the *Caenorhabditis elegans* germline. Dev Biol. 2017;432:222–8.
47. Kocsisova Z, Kornfeld K, Schedl T. Rapid population-wide declines in stem cell number and activity during reproductive aging in *C. elegans*. Development. 2019;146:dev173195.
48. Bolger AM, Lohse M, Usadel B. Trimmomatic: a flexible trimmer for Illumina sequence data. Bioinformatics. 2014;30:2114–20.
49. Dobin A, Davis CA, Schlesinger F, Drenkow J, Zaleski C, Jha S, et al. STAR: ultrafast universal RNA-seq aligner. Bioinformatics. 2013;29:15–21.
50. Li H, Handsaker B, Wysoker A, Fennell T, Ruan J, Homer N, et al. The Sequence Alignment/Map format and SAMtools. Bioinformatics. 2009;25:2078–9.
51. Liao Y, Smyth GK, Shi W. featureCounts: an efficient general purpose program for assigning sequence reads to genomic features. Bioinformatics. 2014;30:923–30.
52. Lun AT, Chen Y, Smyth GK. It's DE-licious: a recipe for differential expression analyses of RNA-seq experiments using quasi-likelihood methods in edgeR. Methods Mol Biol. 2016;1418:391–416.
53. Law CW, Chen Y, Shi W, Smyth GK. voom: precision weights unlock linear model analysis tools for RNA-seq read counts. Genome Biol. 2014;15:R29.
54. McNally K, Audhya A, Oegema K, McNally FJ. Katanin controls mitotic and meiotic spindle length. J Cell Biol. 2006;175:881–91.

ACKNOWLEDGEMENTS

We thank Judith Yanowitz, Peter Boag, and members of the Pocock Laboratory for comments on the manuscript. We thank Hannah Seidel for advice and custom R script for germ cell analysis and for Monash MicroImaging for their support. Some strains were provided by the *Caenorhabditis* Genetics Center (University of Minnesota), which is funded by NIH Office of Research Infrastructure Programs (P40 OD010440).

AUTHOR CONTRIBUTIONS

Conceptualization: WC, SG, and RP; methodology: WC, SKA, SG, and RP; investigation: WC, CT, SKA, and SG; writing—original draft: RP; writing—review and editing: WC, CT, SKA, SG, and RP; funding acquisition: SG, RP; resources: SG and RP; and supervision: SG and RP.

FUNDING

This work was supported by the following grants: NHMRC (GNT1105374 and GNT1137645 to RP, and GNT1161439 to SG), ARC (DP200103293 to RP and DE190100174 to SG), and veski Innovation Fellowship (VIF23 to RP).

COMPETING INTERESTS

The authors declare no competing interests.

ADDITIONAL INFORMATION

Supplementary information The online version contains supplementary material available at https://doi.org/10.1038/s41418-021-00891-z.

Correspondence and requests for materials should be addressed to Sandeep Gopal or Roger Pocock.